Chronoamperometric Evaluation of Several Organic Corrosion Inhibitors by the Hydrogen Permeation Flux

by

Yahya Taqui Al-Janabi

A Thesis Presented to the

FACULTY OF THE COLLEGE OF GRADUATE STUDIES

KING FAHD UNIVERSITY OF PETROLEUM & MINERALS

DHAHRAN, SAUDI ARABIA

In Partial Fulfillment of the
Requirements for the Degree of

MASTER OF SCIENCE

In

CHEMISTRY

June, 1993

Order Number 1355313

Chronoamperometric evaluation of several organic corrosion inhibitors by the measurement of the hydrogen permeation flux

Al-Janabi, Yahya Taqui, M.S.

King Fahd University of Petroleum and Minerals (Saudi Arabia), 1993

U·M·I
300 N. Zeeb Rd.
Ann Arbor, MI 48106

CHRONOAMPEROMETRIC EVALUATION OF SEVERAL ORGANIC CORROSION INHIBITORS BY THE MEASUREMENT OF THE HYDROGEN PERMEATION FLUX

BY

YAHYA TAQUI AL-JANABI

A Thesis Presented to the

FACULTY OF THE COLLEGE OF GRADUATE STUDIES

KING FAHD UNIVERSITY OF PETROLEUM & MINERALS

DHAHRAN, SAUDI ARABIA

In Partial Fulfillment of the
Requirements for the Degree of

MASTER OF SCIENCE

In

CHEMISTRY

JUNE 1993

KING FAHD UNIVERSITY OF PETROLEUM AND MINERALS
DHAHRAN 31261, SAUDI ARABIA

COLLEGE OF GRADUATE STUDIES

This thesis, written by **Yahya Taqui Al-Janabi** under the direction of his Thesis Advisor and approved by his Thesis Committee, has been presented to and accepted by the Dean of the College of Graduate Studies, in partial fulfillment of the requirements for the degree of **MASTER OF SCIENCE IN CHEMISTRY.**

Thesis Committee

G. A. Oweimreen

Dr. G. A. Oweimreen, *Thesis Advisor*

S. J. Lyle

Prof. S. J. Lyle, *Member*

Prof. U. K. A. Klein, *Member*

Dr. A. M. Y. Jaber, *Member*

Department Chairman

Dean, College of Graduate Studies

31st of Aug. 1993

Date

كلية الدراسات العليا
COLLEGE OF GRADUATE STUDIES

بسم الله الرحمن الرحيم

اللهم صلي و سلم على محمد و آله الطيبين الطاهرين

وعلى صحبه المنتجبين

To My Family

ACKNOWLEDGEMENT

Praise be to Allah, Lord of the Universe. May blessings and greetings be upon prophet Mohammed, his posterity, and his companions.

I wish to express my sincere appreciation and gratitude to my Major Advisor and Thesis Committee Chairman Dr. G.A. Oweimreen, who has been a constant source of patient guidance, generous support, and encouragement throughout this study. My thanks and appreciation are extended to the other members of my Thesis Committee, Dr. S.J. Lyle, Dr. U.K.A. Klein, and Dr. A.M.Y. Jaber for their review of my work and for their valuable suggestions and remarks.

My deep thanks are due to the Chemistry Department; Chairman, Faculty, Members, and Staff Members.

I also wish to thank Saudi Aramco for offering me the sponsorship. I am also indebted to Saudi Aramco Laboratories Department and its management personnel for allowing me to use all the facilities available in the Department to conduct this work. Special thanks are forwarded to Mr. M.A. Al-Houtan, the Manager of the Saudi Aramco Laboratories Department, and Dr. A.L. LewisII, my mentor and advisor at Saudi Aramco.

Finally, a word of appreciation should go to my family and friends and every person who helped me in this regard.

TABLE OF CONTENTS

LIST OF TABLES

LIST OF FIGURES

خلاصة الأطروحه

أسم الطالب: يحيى تقي الجنبي

عنوان الدراسه: التقييم الكرونوأمبيروميتري لبعض كابحات التآكل العضويه بقياس النفاذ التدفقي للهيدروجين

حقل التخصص: الكيمياء

تاريخ الدرجة العلميه: ذو الحجه 1413 هجريه (يونيو 1993 م)

لقد تم بنجاح تصميم، و بناء، و استخدام جهازا كهروكيميائيا لقياس نفاذية الهيدروجين. إن التوافق الممتاز بين قيم معاملات إنتشار ذرات الهيدروجين في الحديد التي حصلنا عليها و بين القيم التي حصل عليها باحثون آخرون، برهن على إمكانية التعويل على هذا الجهاز للقيام بالقياسات اللازمه. كما لوحظت حدبه متميزه في بعض منحنيات نفاذية الهيدروجين. و نقترح أن هذه الحدبه ناتجه عن إحتباس الهيدروجين في مواطن متعدده سوى الفجوات و الفجوات المجهريه.

لقد أستخدم هذا الجهاز الكهروكيميائي لدراسة فعالية كل من ثنائي الأيثانول الأميني (Diethanolamine)، و المورفلين (Morpholine)، و ثلاثي الأيثانول الأميني (Triethanolamine)، و ثنائي الأمين الأيثيلي (Ethylenediamine)، و ثنائي الأمين الهيكساميثيلي (Hexamethylene diamine)، في كبح عملية دخول الهيدروجين في الحديد. وثبت أن ثنائيات الأمينات أكثر فعالية من أحاديات الأمينات، و كذلك أن العلاقة بين تركيز المواد العضويه الآنفة الذكر ومدى زيادة الكبح علاقة غير خطيه.

و تم الوصول الى أن قدرات أحاديات الأمينات على الكبح متقاربه عند الحد الأعلى للتركيز (0,01 مولار) و متفاوته عند الحد الأدنى للتركيز (5×10^{-5} مولار) حسب الترتيب الآتي: ثلاثي الأيثانول الأميني > المورفلين > ثنائي الأيثانول الأميني. كذلك أن قدرات ثنائيات الأمينات على الكبح متقاربه عند حدها الأعلى للتركيز (5×10^{-3} مولار) و متفاوته عند الحد الأدنى للتركيز (5×10^{-5} مولار) حسب الترتيب الآتي: ثنائي الأمين الهيكساميثيلي > ثنائي الأمين الأيثيلي.

درجة الماجستير في العلوم

جامعة الملك فهد للبترول و المعادن

الظهران، المملكه العربيه السعوديه

يونيو 1993 م

THESIS ABSTRACT

Name of Student: YAHYA TAQUI AL-JANABI

Title of Study: CHRONOAMPEROMETRIC EVALUATION OF SEVERAL ORGANIC CORROSION INHIBITORS BY THE MEASUREMENT OF THE HYDROGEN PERMEATION FLUX

Major Field: CHEMISTRY

Date of Degree: JUNE 1993

An electrochemical hydrogen permeation measurement system was designed, constructed and successfully used. The good agreement between the values of the diffusion coefficients for the hydrogen atoms in steel obtained by us and those obtained by other workers established the reliability of our system. A characteristic hump was observed in several hydrogen permeation curves. We propose that this hump is due to the trapping of hydrogen at sites other than voids and microvoids.

This electrochemical system was adapted to study the effectiveness of diethanolamine (DEA), morpholine (MOR), triethanolamine (TEA), ethylenediamine (EDA), and hexamethylene diamine (HMDA) in inhibiting the entry of hydrogen atoms into steel. The diamines were found to be more effective than the monoamines, and a nonlinear relationship was observed between the increase of inhibition and the concentration of the amines studied.

The inhibiting abilities of the monoamines were similar at the higher concentration limit (0.01M) and followed the trend TEA > MOR > DEA at the low concentration limit (5×10^{-5}M). For the diamines the inhibiting abilities were also similar at their high concentration limit (5×10^{-3}M) and followed the trend HMDA > EDA at the low concentration limit (5×10^{-5}M).

MASTER OF SCIENCE DEGREE

KING FAHD UNIVERSITY OF PETROLEUM AND MINERALS
Dhahran, Saudi Arabia

June 1993

CHAPTER 1

INTRODUCTION

The entry of hydrogen atoms into iron-base alloys is an undesirable process because it damages the physical and mechanical properties of the metal. Certain environments substantially increase the amount of hydrogen atoms that can enter the metal. One example is the "sour environment" arising from hydrogen sulfide in the presence of moist or water. Hydrogen sulfide corrosion has been identified[1] as a major contributor to the premature failure of various materials in the oil industry.

While hydrogen sulfide corrosion has been known at least as early as 1948,[2] its impact on the oil industry[3] has become even more appreciable in the last ten to fifteen years. During this period oil emulsions with higher water content were treated at higher production temperatures.[4] At these higher temperatures H_2S solubility is reduced and the thermal decomposition of sulfur compounds[4] is enhanced. Both factors tend to increase the released H_2S.

The types of equipment that can be damaged by H_2S in the oil industry include:[4] transport pipelines and tankers, equipment for recovering and cleaning natural gas, tanks

and reservoirs, gas fractionation units, hydrocracking of sulfurous oils, and equipment for compressing and transferring natural gases.

Amine chemical inhibitors (*vide infra*)[1] are frequently applied to mitigate hydrogen sulfide corrosion and hydrogen entry. Studying the effect of amine chemical inhibitors on hydrogen entry is of both academic and technological interest. Areas to which this study is relevant include physical electro- and organic chemistry and surface science. In technology, such studies assist significantly in the design of a cost-effective inhibition program.

An electrochemical method (*vide infra*) used to study hydrogen permeation rates and to determine hydrogen diffusion coefficients in metals was adapted for this particular research problem; namely the study of the effects of certain organic amines on hydrogen entry into steel. To achieve this objective, an electrochemical hydrogen permeation system had to be designed, constructed, and optimized.

[1] This term will be used whenever more information will be given later in this write-up.

CHAPTER 2

HYDROGEN DAMAGE

Hydrogen damage is a general term which refers to the mechanical deterioration of a metal caused by the presence of hydrogen. Atomic hydrogen is capable of diffusing through steel and other metals. The molecular form of hydrogen cannot diffuse through metals. Thus, hydrogen damage results only from the atomic form of hydrogen.

This chapter is divided into four sections. In the first section, the four types of hydrogen damage are discussed briefly. In the other three sections, the following issues are addressed: the steps involved in the production of hydrogen atoms from hydronium ions in contact with a metal surface (section 2.2), the process of hydrogen atom entry into steel (section 2.3), and the role of hydrogen sulfide in promoting hydrogen entry (section 2.4). Since the inhibition of hydrogen entry is a surface reaction, the behavior of hydrogen atoms inside the steel lattice has not been emphasized in this write-up.

2.1 Types of Hydrogen Damage

Hydrogen damage takes several forms,[5] which are interrelated to different

degrees. These are:

(i) *Sulfide Stress Cracking* (SSC) which occurs when hydrogen interacts with high-strength (tensile strength >620 MPa) and/or high hardness (hardness >200 Brinell, BHN) steels.

(ii) *Hydrogen Blistering* where the damage occurs parallel to the surface of the steel plate and is caused by the increase in pressure resulting from the accumulation of molecular hydrogen in non-metallic inclusions and other discontinuities located at the same depth in the steel.[2]

(iii) *Step-wise cracking* takes place when the inclusions are short and at varying depths within the thickness of the steel. The step-wise cracks may produce a blister, or link a series of blisters up to the surface to relieve the pressure.

(iv) *Stress-Oriented Hydrogen-Induced Cracking* - In this type, the hydrogen pressure within fissures causes them to link thereby forming a through-thickness crack that could reach a length of 38 cm.[5]

2.2 Hydrogen Evolution Reactions

Hydrogen evolution reactions are believed to occur in the following consecutive

steps:[6-8]

Step-1 Hydrated protons, H_3O^+, are transported to the double layer of a metal surface.

Step-2 Hydrated protons are desolvated in the vicinity of the double layer and the carrier water molecules depart to the bulk solution.

Step-3 Protons are adsorbed at the metal surface

$$H^+_{(aq)} + M \rightarrow MH^+_{ads} \qquad [1]$$

Step-4 The adsorbed protons are reduced (discharged or electronated) to adsorbed hydrogen atoms.

$$MH^+_{ads} + e^- \rightarrow MH_{ads} \qquad [2]$$

Step-5 The recombination of hydrogen atoms. Two mechanisms have been proposed for this step:

a) Atom-atom recombination (also called Tafel or chemical recombination). According to this mechanism two adjacent adsorbed hydrogen atoms combine to form a hydrogen molecule.

$$MH_{ads} + MH_{ads} \rightarrow 2M + H_2 \qquad [3]$$

b) Atom-ion recombination (also called electrodic or electrochemical recombination) involves the combination of a proton and an adatom to form a hydrogen molecule.

$$MH_{ads} + H^{+}_{(aq)} + e^{-} \rightarrow M + H_{2\,(ads)} \qquad [4]$$

or

$$MH_{ads} + H^{+}_{(aq)} + M(e^{-}) \rightarrow 2M + H_{2\,(ads)} \qquad [5]$$

Step-6 Desorption of the hydrogen molecule.

Step-7 Evolution of coalesced hydrogen molecules.

In the recombination step, the surface concentration of adsorbed H must be high for the probability of collision between aqueous hydrogen ions and adsorbed hydrogen atoms to be high, while the atom-atom recombination reaction can proceed at low coverage.[6] A competing process with the hydrogen recombination step is hydrogen absorption by the metal. This process will be discussed further in the next two sections.

The steps that would affect the overall reaction rate are the discharge step (step 4), one of the recombination steps (step 5a or 5b), and the desorption step (step 6). The desorption step is usually invoked in the recombination step because of the weak affinity

for hydrogen molecules to chemisorb to the metal. Thus either of the two steps, discharge followed by chemical or electrochemical recombination, or both of them may be rate-determining.

The mechanism of the hydrogen evolution reaction on iron in, for example, an acetate buffer of pH 3.6 and in 0.1N H_2SO_4 solutions, was found[9] to be a slow discharge, followed by atom-atom recombination at low overpotentials, and atom-ion recombination at high overpotentials (>600 mV).

2.3 Hydrogen Entry in Iron (or Steel)

In their 1966 paper McBreen et al.[10a] trace the discovery of the permeability of iron to hydrogen atoms to Cailletet[10b] who published his work in 1864. Two models were proposed for hydrogen entry: the first assumes that hydrogen enters in the same elementary form (atomic or nascent) as it exists on the metal surface, and in the second model, the hydrogen ion is discharged and passes directly into the metal with no intermediate steps.[7] In the first model there will be a competition between the recombination and the absorption reactions. While in the second model, such competition will not exist.

Absorbed or dissolved hydrogen creates a concentration gradient between the surface where hydrogen enters and the interior of the metal. The net effect of this

concentration gradient is to make the adsorbed hydrogen diffuse into the metal.[11] Hydrogen permeation flux through a metal is a function of its solubility and diffusion coefficient in that metal.

The mechanism for hydrogen diffusion seems to vary from one metal to another.[12] For iron, it was found[13,14] that the diffusion coefficient for hydrogen was the same for both poly-crystalline and single-crystal structures. This suggested a diffusion process which depends on the ease with which the metal-metal bond stretches as a hydrogen atom jumps between neighboring interstitial sites. This led Bockris et al.[15] to predict a relation between the diffusion coefficient and the latent heat of sublimation of the metal. The diffusion coefficient was found[15] to decrease with increasing latent heat of sublimation for the series Fe, Pd, Ni, Pt, Zr, Mn, Ti, and Ta, thereby confirming their prediction. Namboodhiri and Nanis[16] found that the diffusivity of hydrogen in iron is directly proportional to the hydrogen concentration in it.

Hydrogen diffusion paths could be interrupted by the presence of dislocations,[17] solid-solid interfaces,[17] microcrack surfaces in cold worked steels,[17] vacancies[14] or microvoids,[11] grain boundaries,[18] and solute atoms.[15,18] A tensile stress (external or residual) field in metals increases hydrogen solubility,[11] i.e. stretching a metal leads to increased hydrogen absorption, and all imperfections in crystals are regions of distortion or strain. For example when hydrogen atoms encounter a microvoid (which can reach 100Å[11] across) they recombine to form hydrogen molecules and pressure builds up to

the extent that the metal is plastically deformed.[11] It was estimated[11] that the pressure might reach up to 10^5 to 10^7 atm inside the microvoid. These are called trapping sites, and the process of trapping could be reversible (to different extents) or irreversible.[19]

2.4 The Role of Hydrogen Sulfide

The mechanism of the reaction for the evolution of molecular hydrogen on iron or steel surfaces is believed to be a coupled discharge-recombination mechanism.[20]

$$H_3O^+ + e^- + Fe \xrightarrow[(slow)]{k_1} FeH_{ads} + H_2O \qquad [6]$$

$$FeH_{ads} + FeH_{ads} \xrightarrow{k_2} 2Fe + H_2 \qquad [7]$$

$$FeH_{ads} \underset{k_{-3}}{\overset{k_3}{\rightleftarrows}} FeH_{abs} \qquad [8]$$

Certain species enhance hydrogen entry. These species were given two generic terms: "promoters" when the enhancement is by promotion of the hydrogenation of the metal, or "poisoners" when the enhancement results from the poisoning or inhibition of the hydrogen evolution reaction on the metal surface.[21] Therefore, promoters, somehow, increase the energy barrier for the recombination step and favor the competing absorption step. Several promoters were identified: sulfur,[2] arsenic,[2,21] selenium,[2] tellurium,[2] antimony,[2] phosphorus,[2] cyanide and amino butyrate anions[22]. Hydrogen sulfide has the dual property of being a source of hydrogen and a promoter.

2.4.1 Hydrogen Sulfide-Steel Reactions

In aqueous acidic sulfide solutions, the following cathodic reactions were proposed:[4,23]

$$H^+ + e^- \rightarrow H_{ads} \rightarrow 1/2\ H_2 \qquad [9]$$

$$H_2S + e^- \rightarrow HS^- + 1/2\ H_2 \qquad [10]$$

$$H_2S + 2e^- \rightarrow S^{2-} + H_2 \qquad [11]$$

While the following two processes were suggested for the anodic reaction:[4,23-25]

1. Dissolution with precipitation:

$$Fe \rightarrow Fe^{2+} + 2e^- \quad [12]$$

$$Fe^{2+} + S^{2-} \rightarrow FeS \quad [13]$$

2. Direct film formation:

$$Fe + HS^- \rightarrow Fe(SH)_{ads} + e^- \quad [14]$$

$$Fe(SH)_{ads} \rightarrow FeS + H^+ + e^- \quad [15]$$

Acceleration of anodic processes in the presence of H_2S was explained by the following reactions:[4]

$$Fe + H_2S + H_2O \rightleftarrows (FeHS^-)_{ads} + H_3O^+ \quad [16]$$

$$(FeHS^-)_{ads} \rightarrow FeHS^+ + 2e^- \quad [17]$$

$$FeHS^+ + H_3O^+ \rightleftarrows Fe^{2+} + H_2S + H_2O \quad [18]$$

Reactions [16]-[18] show the autocatalytic effect of H_2S on iron dissolution. According to these reactions, the concentration of hydrogen sulfide will be constant since it is consumed in reaction [16] and regenerated in reaction [18]. Another suggested reaction

assumes almost a constant concentration of $(FeSH)_{ads}$ catalyst at the surface:[4]

$$Fe(FeSH)_{ads} \rightarrow (FeSH)_{ads} + Fe^{2+} + 2e^{-} \qquad [19]$$

Depending on the pH, $FeHS^{+}$ would hydrolyze according to reaction [18], or transfers to the sulfide:[26]

$$FeHS^{+} + H_2O \rightarrow FeS + H_3O^{+} \qquad [20]$$

Moreover, oxide films on the metal surface can be more easily converted into sulfides than the metal base:[25]

$$FeO + H_2S \rightarrow FeS + H_2O \qquad [21]$$

2.4.2 The Sulfide Film

The pH,[23] the temperature,[27] the dynamic state[24] and the composition of the solution govern the type and protectiveness of iron sulfide scales that form on steel surfaces. For a stirred, H_2S-saturated distilled water (pH ~4) at room temperature in contact with an iron or steel surface, the most common corrosion product is mackinawite (tetragonal FeS_{1-x}).[24] The mackinawite layer was defined[24] as a cracked, porous base layer which does not passivate the surface of the metal (see section 3.2 for a modified view of the sulfide layer). For the formation of the mackinawite base layer, reaction [20] can be written as:[24]

$$FeHS^+ + (1\text{-}x)\ H_2O \rightarrow FeS_{1-x} + x\ HS^- + (1\text{-}x)\ H_3O^+ \qquad [22]$$

where $0 < x < 1$.

2.4.3 The Promotion Mechanism

The mechanism by which H_2S and/or HS^- and/or FeS_{1-x} promote hydrogen entry (absorption) is not very clear. However, several observations and propositions are worthy of mention. These are:

(i) H_2S autocatalyses Fe anodic dissolution by reactions [16] - [19].

(ii) Adsorption of HS^- ions is accompanied by the segregation of sulfur on the surface within grains or at their boundaries. Sulfur then diffuses independently into iron and steel to a depth of up to 120 μm[4] normal to the surface.

(iii) HS^- adsorption stimulates the discharge of H^+ ions and accelerates the cathodic process, thereby reducing hydrogen overvoltage, η_H.[4,23]

(iv) The promoter species adsorb or deposit first at the more energetic sites, leaving hydrogen to adsorb at less energetic sites,[21] and this will account for a lowering in η_H as well.

(v) Adsorption of HS^- reduces the hydrogen-metal bond energy due to the formation of a direct Me-HS^- bond.[4,21]

(vi) A potential difference develops, between the sulfide films and the steel, creating a galvanic couple.[4]

The overall effect of promoters (or poisoners) is the lowering of the energy of the metal-hydrogen bond and in turn the lowering of the activation energy of the

$$H_{ads} \rightarrow H_{abs}$$

process, thereby increasing the proportion of absorbed H atoms.

CHAPTER 3

AMINE INHIBITORS AND THE ELECTROCHEMICAL PERMEATION TECHNIQUE

This chapter consists of two main parts. The first part, which is divided into three sections, deals with amine corrosion inhibitors. To understand the behavior of organic amine inhibitors, a brief theoretical introduction is given in the first section. In the second section, the specific case of inhibiting the damage induced by hydrogen sulfide is reviewed. Then, the first part is concluded by presenting some of the previous work conducted on the amines corrosion inhibitors investigated in this study. The second part deals with the electrochemical hydrogen permeation measurement system (section 3.4) adopted in this study.

3.1 Organic Amine Inhibitors

These are nitrogen-bearing organic compounds which demonstrated inhibitive action against corrosion processes. Their inhibition efficiency is determined, basically, by comparing the extent of corrosion in their presence and in their absence.

3.1.1 Inhibition Mechanisms

Although different inhibition mechanisms have been identified[28] (either directly or by studying their effect) for inhibitors in general, several of these mechanisms could occur simultaneously. These mechanisms can be broadly classified into two main types.

(i) **Interface Inhibition:** In this type of inhibition,[29] the inhibitor is directly adsorbed on the metal surface, forming a thin two-dimensional (2-D) film. This type can be further subdivided into non-selective and selective physisorption and chemisorption. In *non-selective* physisorption, which is also called geometrical blocking[29] or screening[30] the adsorption is rapid and reversible, and the inhibitor which is indifferent to the nature of the adsorbent interacts with the surface via Van der Waal or electrostatic forces that lead to a relatively high degree of coverage. *Selective* physisorption, also called deactivating coverage,[31] involves[29] selective blockage of active sites at the metal surface by an indifferent inhibitor at relatively low coverages. Chemisorption, also called reactive coverage,[31] is characterized by a specific and slow[30] adsorption that is not completely reversible[28] and involves charge sharing or transfer.

(ii) **Interphase Inhibition:** A three-dimensional (3-D) layer[29] emerges on the metal surface[32] resulting from, for example, the chemical reaction of an inhibitor with corrosion products to form organometallic complexes.

3.1.2 Factors Influencing Inhibitor Efficiency

Several structural and chemical factors determine the effectiveness of an inhibitor. For organic amines as inhibitors the following characteristics were identified.

(i) If chemisorption is involved in the inhibition process its contribution to the inhibition efficiency will increase as the electronic density[33] or electron donation ability of the reaction center, nitrogen, increases.

(ii) An increase in the carbon chain length of an amine inhibitor will enhance[34] the inhibition efficiency. This could be attributed to an increase in the electronic density at nitrogen due to inductive effects,[28] an increase in the coverage ability,[35] hydrophobicity,[34] and polarizability[28] and a decrease in the solubility[34] of the inhibitor.

(iii) Inhibition efficiency will be affected by the degree of overlap between the inhibitor molecular orbital and the metal d-orbital,[36] and the ability of the inhibitor to complex with the metal[37] itself or the corrosion products.[38]

(iv) The formation of a compact layer,[37] e.g. cross-linking, enhances inhibitor performance.

3.2 Inhibition of H_2S-Damage

Organic amines were found[38] to be highly effective inhibitors in corrosion systems where H_2S is present.

Iofa[39] suggested the following reaction steps to explain H_2S catalytic action in accelerating the anodic corrosion reaction:

First, $H_2S + H_2O \rightleftarrows H_3O^+ + HS^-$ [22]

$Fe + HS^- \rightleftarrows Fe\,(HS^-)_{ads}$ [23]

or $Fe + H_2S + H_2O \rightleftarrows Fe\,(HS^-)_{ads} + H_3O^+$ [24]

Then, $Fe(HS^-)_{ads} \rightarrow Fe(HS)_{ads} + e^-$ [25]

$Fe\,(HS)_{ads} \rightarrow FeHS^+ + e^-$ [26]

$FeHS^+ + H_3O^+ \rightarrow Fe^{2+} + H_2S + H_2O$ [27]

Iofa suggested that $Fe(HS^-)_{ads}$ is responsible for the accelerated anodic dissolution (reactions [25]-[27]) and for increasing hydrogen entry by weakening the metal-hydrogen bond through its participation with H_3O^+ ions to give $Fe(H\text{-}S\text{-}H)_{ads}$, that in turn lead to

the easy reduction of protons. This latter process can be represented[39] by the following reactions;

$$Fe(HS^-)_{ads} + H_3O^+ \rightleftarrows Fe(HS\text{-}H)_{ads} + H_2O \qquad [28]$$

$$Fe(HS\text{-}H)_{ads} + e^- \rightarrow Fe(HS^-)_{ads} + H_{ads} \qquad [29]$$

Then adsorbed hydrogen atoms will either recombine to form hydrogen molecules, or diffuse into the metal. On the basis of these arguments, Iofa[39] explained the good inhibitive properties of organic amines in the presence of H_2S as follows:

(i) Adsorption of the protonated inhibitor, e.g., RNH_3^+ on iron,[30] is substantially facilitated by $Fe(HS^-)_{ads}$.[34]

(ii) As a result of step (i) $Fe(HS^-)_{ads}$ will be deactivated, or its action, i.e. reactions [25]-[29], will be retarded.

(iii) Adsorbed inhibitors would increase the ohmic drop across the double layer, and therefore increase the hydrogen overvoltage, η_H.

Donahue et al.[40] proposed a mechanism for the complexation of aniline and aniline derivatives, designated by I, to adsorbed iron hydroxide:

$$Fe(OH)_{ads} + n\,I \rightleftarrows [(FeOH).\,I_n]_{ads} \qquad [30]$$

$$[(FeOH).I_n]_{ads} \rightarrow [(FeOH).I_n]^+ + e^- \qquad [31]$$

In this case, aniline or an aniline derivative stimulates corrosion since the complex $[(FeOH).I_n]^+$ is water soluble.[40]

On the other hand, there are cases where the complex produced will form a protective layer that inhibits corrosion. Rozenfel'd et al.[32,41,42] and others[34,43,44] concluded that, in the presence of H_2S, the emergence of a protective phase layer is the main contributor to the enhanced performance of the organic amines. For iron in an H_2S-saturated aqueous system, Rozenfel'd et al.[42] observed (using X-ray diffraction, Auger spectroscopy, ESCA and mass spectroscopy), that initially a high density, fine crystalline protective layer - mackinawite - forms but with the passage of time its structure changes to a less protective coarse crystalline layer with a large number of macrodefects. Under steady-state conditions[42] an equilibrium exists between the fine and coarse crystalline forms of the mackinawite base layer. Organic amine inhibitors react[41] with iron, H_2S, and/or corrosion products, to form organometallic complexes which prevent[43] the recrystallization of the mackinawite base layer and preserve its protective properties. Panov et al.,[45] using photoelectronic spectroscopy, observed the presence of the mackinawite layer on an iron specimen pre-exposed to an amine inhibitor, after being placed in the H_2S-containing media.

Rozenfel'd et al.[42] did not support any participation of the adsorption mechanism

in this system (iron-H_2O-H_2S-amine inhibitor) proposed by Iofa. However, Iofa[39] mentioned that his suggested processes would be valid under low H_2S and inhibitor concentrations. Moreover, recent studies[43,45] regard inhibition by adsorption as a secondary process. Therefore, the H_2S and inhibitor concentrations, dynamic conditions, temperature, and time would determine extents of the contribution of the protective phase layer and the adsorption mechanisms to the inhibition process.

3.3 Chemicals Studied

Typical organic amine compounds that were studied for the inhibition of hydrogen entry, along with the literature reference numbers, are given in Table 1. Rozenfel'd et al.[41] prepared and tested an inhibitor, on bench and industrial scales, for both corrosion and hydrogenation (hydrogen damage) inhibition. Dioctylaminopropionitrile[49], which is the main component in this inhibitor, prevented hydrogenation by film formation, blocking, and hydrophobicity.

In this study, used or proposed chemical inhibitors were investigated. These are diethanolamine,[29] triethanolamine,[28,35,50] morpholine,[52,53] ethylenediamine,[35,50,54] and hexamethylene diamine[54] (see Appendix for general information about these chemicals).

TABLE 1

Typical Amines Studied for the Inhibition of Hydrogen Entry, along with their Literature Reference Numbers.

Organic Amine Studied	Reference No.
Valeronitrile	46
Benzonitrile	46
Naphthonitrile	46
Pyridine derivatives	47
Primary aliphatic amines	34
Amidoamines	34
2-Phenyl-2-imidazolines	34,51
Mono-,di-, and tri-allyl amines	38
Di-ortho aminobenzene disulfide	48
Dioctylaminopropionitrile	49
Octadecylamine	43
Benzimidazole derivatives	55
Mono-and tri-ethanol amines	50
Ethylenediamine	50

Singh et al.[50] investigated the effect of triethanolamine (TEA) and ethylenediamine (EDA), among other amines, as inhibitors for the corrosion and the hydrogen absorption of API-45 grade steel in a sour solution using gravimetric (weight-loss), hydrogen-estimation, electrochemical (potentiostatic), and techniques involving the determination of the tensile strength of materials. EDA was found[50] to be a better inhibitor for both corrosion and hydrogen absorption than TEA. Inhibition mechanisms suggested[50] were chemisorption, interphase, and the displacement of H_2S molecules or ions from the metal surface by the inhibitor molecules.

Raicheva et al.[35] studied the effect of monoethanolamine (MEA), TEA, EDA, and morpholine (MOR), among various nitrogen- and sulfur-containing inhibitors, on the corrosion of iron and steel using gravimetric and electrochemical (potentiostatic, polarization resistance, and impedance method) techniques. By evaluating the mean values of the inhibitor activity obtained by the different methods, they found[35] the following sequence of decreasing inhibition efficiency: EDA > MEA > MOR ≥ TEA.

Jacklin[52,53] recommended the use of morpholine to control corrosion in the steam-condensate system of power generating utilities. According to him, morpholine neutralizes carbon dioxide (a decomposition product of bicarbonates and carbonates in the feed water or evaporator system) and maintains a pH ~9 which appreciably retards the corrosion process.

3.4 The Electrochemical Hydrogen Permeation Technique

3.4.1 Introduction

The quantity of absorbed hydrogen and corrosion rate are not directly related,[41] i.e. high corrosion rates are not necessarily accompanied by high hydrogen permeation rates, or vice versa. The evaluation techniques of corrosion inhibitors cannot be used to determine the effect of the inhibitor on hydrogen penetration into the metal. Methods used to study hydrogen penetration include:[28]

(i) Calculating the amount of hydrogen penetrated by determining the amount of hydrogen evolved, e.g. by gas-volumetry, and the amount of dissolved iron, e.g. by colorimetry.

(ii) Examining blisters,[48] formed because of hydrogen absorption, by microscopic examination.

(iii) Determining the brittleness of metal samples caused by hydrogenation (indices used can be the breaking load, bending angles, maximum number of rotations or torsions of a metal wire before breakage).

(iv) Determination of absorbed hydrogen by vacuum extraction[41] or by hot

extraction[50] using gas chromatography with argon as carrier gas.

(v) Electrochemical determination of the permeating hydrogen atoms (*vide infra*).

3.4.2 The Principle of the Electrochemical Method

Devanathan and Stachurski[9,22,56] constructed and characterized an electrochemical permeation system for the measurement of hydrogen diffusion through metals. A brief description of this method is given below. A detailed description could be found elsewhere.[9,10,22,56-59]

The Devanathan-Stachurski apparatus, or the Devanathan-Stachurski-Bockris apparatus,[60] consists of two compartments, each containing a counter electrode and a reference electrode, separated by a metal membrane (the working electrode to be studied). On the charging side, a steady-state concentration of adsorbed hydrogen atoms on the surface of the membrane is maintained by cathodic polarization using a glavanostatic circuit. On the permeation or measurement side, a zero concentration of adsorbed hydrogen atoms on the other surface of the membrane is maintained by anodic polarization, using a potentiostatic circuit.

The anodic potential in the measurement side is set so that absorbed hydrogen atoms from the charging side will be driven out to the anodic side and oxidized at the

instant of exit. Thus, the current in the anodic potentiostatic circuit is by Faraday's laws a direct measure of the instantaneous rate of permeation of hydrogen through the metal membrane. The anodic side of the metal membrane, e.g. iron or steel, is electroplated with a very thin layer of palladium to prevent anodic dissolution or passivation without affecting the permeation rate of the hydrogen atoms. Moreover, palladium has a much higher solubility for hydrogen than iron[63], and thereby reduces the probability of the recombination of hydrogen atoms on the exit side. This kind of experiment is called chronoamperometry, because current (or current density) is recorded as a function of time.

Kumnick and Johnson[64,65] and others[66,67] were able to modify this technique and measure hydrogen permeation from a gas phase (the charging side) through iron electroplated with palladium from both sides. The measurement compartment was unaltered. Berman et al.[68] simplified the anodic potentiostatic circuit by replacing the counter electrode and the reference electrode normally used in the Devanathan-Stachurski apparatus by Ag/Ag_2O or Ni/NiO electrodes to maintain sufficient potential to oxidize hydrogen atoms arriving at the exit side.

3.4.3 Diffusion Theory of the Electrochemical Hydrogen Permeation Technique

The distribution of hydrogen atoms in an ideal homogeneous steel can be derived[61] from the solution of Fick's second law;

$$\partial c/\partial t = D\ \partial^2 c/\partial x^2 \qquad [32]$$

where c is concentration, t is time, D is diffusion coefficient, and x is distance. The initial and boundary conditions established by the electrochemical permeation method for a membrane of thickness L, are:[10,15]

$$c = c_o\ ;\ x = 0\ \ ;\ t\ \geq\ 0,$$

$$c = 0\ \ ;\ x = L\ \ ;\ t\ \begin{matrix}< \\ > \end{matrix}\ 0, \text{ and}$$

$$c = 0\ \ ;\ 0 < x < L\ ;\ t\ \leq\ 0,$$

where c_o is a constant concentration.

Several methods were used to derive an expression to calculate D, the hydrogen diffusion coefficient, from hydrogen permeation data.

(i) The Time-to-Breakthrough Method:[56]

$$D = \frac{L^2}{15.3\ t_b}\ , \qquad [33]$$

where t_b, the breakthrough time, is found by extrapolating the linear portion of the initial

rising current transient to J (the flux) = 0, while the time of commencement of cathodic charging is taken to be $t = 0$.

(ii) **The Time-Lag Method:**[56]

$$D_{0.63} = \frac{L^2}{6\,T_{lag}} \cdot \qquad [34]$$

T_{lag} is the time, from $t = 0$, that corresponds to the point on the permeation curve at which $J = 0.6299 J_\infty$ (J_∞ is the steady-state value).

(iii) **The Fourier Method.**[10,56,61] The rising transient is given by Equation [35].

$$\frac{J}{J_\infty} = 1 - 2 \exp\{-\frac{\pi^2 D\, t}{L^2}\} \,, \qquad [35]$$

rearranging gives

$$1 - \frac{J}{J_\infty} = 2 \exp\{-\frac{\pi^2 D\, t}{L^2}\} \,, \qquad [36]$$

and taking the natural logarithm

$$\ln(1 - \frac{J}{J_\infty}) = \ln 2 - \frac{\pi^2 D\, t}{L^2} \cdot \qquad [37]$$

From a plot of $\ln(1 - \frac{J}{J_\infty})$ against t, D can be obtained from the slope, and the intercept should be ln 2. This equation can be used for $J \geq 0.3\, J_\infty$.

(iv) The Laplace method:[10,61] Via a Laplace transformation Fick's second law leads to the relation

$$\frac{J}{J_\infty} = \frac{2}{\pi^{1/2}} \frac{L}{(Dt)^{1/2}} \exp\left\{ - \frac{L^2}{4Dt}\right\} , \qquad [38]$$

that holds for $J \leq 0.965\, J_\infty$.

Rearranging Equation [38], gives

$$Jt^{1/2} = \frac{2L\, J_\infty}{\pi^{1/2}\, D^{1/2}} \exp\left\{ - \frac{L^2}{4Dt}\right\} , \qquad [39]$$

and taking the natural logarithm

$$\ln(Jt^{1/2}) = constant - \frac{L^2}{4Dt} , \qquad [40]$$

where the constant is $\ln\{ 2LJ_\infty/(\pi^{1/2}D^{1/2}) \}$. From a plot of $\ln (Jt^{1/2})$ versus t^{-1}, D can be obtained from the slope and from the intercept. Using this method McBreen et al.[10] showed that if t is the time at which $J = 0.83\, J_\infty$ then

$$D = 0.25\, L^2 / t \qquad [41]$$

and that if $t_{1/2}$ is the time at which $J = 0.5\, J_\infty$[10, 61] then

$$D_{0.5} = 0.138\, L^2/t_{1/2}, \qquad [42]$$

McBreen et al.,[10] and others,[58] also showed that

$$c_o = \frac{J_\infty\, L}{D} , \qquad [43]$$

where c_o is the concentration of hydrogen atoms at the surface of the membrane.

3.4.4 Inhibitor Evaluation Using the Electrochemical Permeation Technique

The electrochemical permeation technique was used to study the effect of chemical inhibitors on reducing the amount of permeating hydrogen which is directly related to the hydrogen surface coverage, θ_H.[46]

Bockris et al.[46] studied the extent of inhibition of hydrogen entry into α-iron in the presence of valeronitrile, benzonitrile, and naphthonitrile in acidic (0.1N H_2SO_4) solutions, by plotting $J_\infty(\mu A/cm^2)$ versus different cathodic potentials at different inhibitor concentrations. They suggested that these chemicals reduced hydrogen entry by vertical adsorption and thereby retarding the hydrogen transportation step (because of steric hindrance), increasing η_H, and consequently decreasing θ_H, which was ultimately reflected in the measured hydrogen permeation flux. Antropov et al.[47] reported the simultaneous measurement of hydrogen permeation and corrosion rate to study the effectiveness of pyridine derivatives which demonstrated good hydrogen inhibition properties.

Martin[51,69] applied the basic principle of the Devanathan-Stachurski apparatus to construct a probe for the measurement of both hydrogen permeation and corrosion rate (by the linear polarization technique). This probe was used in the laboratory and in the field for the evaluation of hydrogen permeation inhibitors (e.g. imidazoline derivatives,

a sulfurated organic phosphorus compound, and a sulfurated hydrocarbon compound) in sour environments.

Jiashen and Jingamo[70] used the electrochemical permeation technique to investigate the efficiency of imidazoline and organic phosphate ester, among other inhibitors, in inhibiting hydrogen entry into a steel exposed to H_2S-bearing drilling mud, and found that imidazoline is a better hydrogenation inhibitor than the other compounds.

In this study we used the electrochemical hydrogen permeation measurement technique to study the effect of diethanolamine (DEA), morpholine (MOR), triethanolamine (TEA), ethylenediamine (EDA) and hexamethylene diamine (HMDA) on the hydrogen entry process into a mild steel (API A106 grade B) working electrode exposed to a hydrogen sulfide-saturated distilled water solution. The Diamines were found to be more effective in inhibiting the hydrogenation process than the monoamines. The effectiveness of inhibition for DEA, MOR and TEA were comparable at the high concentration limit and followed the trend: TEA > MOR > DEA, at the low concentration limit. The effectiveness of inhibition for EDA and HMDA were also comparable at their high concentration limit and followed the trend: HMDA > EDA, at the low concentration limit. Using this method, the effect of the amines on the hydrogen entry process was directly studied.

CHAPTER 4

EXPERIMENTAL

4.1 The Measurement System

The experimental conditions chosen provide a means for comparing the inhibiting behavior of the amine compounds studied and imitate, as closely as possible, the real life conditions of industrial corrosion.

4.1.1 Selection of the Corrosive Medium

Sour environments in the petroleum industry are usually characterized by their relatively low pH values, the absence of oxygen, and by their salinity. To study the inhibiting behavior of the amine compounds without the interference of any other species, a deareated, H_2S-saturated distilled water (pH $\sim$4) at room temperature was chosen as the corrosive medium. The solution was continuously stirred to prevent concentration polarization.

4.1.2 Selection of the Membrane Material

The type of the steel selected for this study is used in sour environments in the petroleum industry and resists hydrogen damage. Membrane samples, whether bare or electroplated with palladium on one side, were machined from API A106 grade B, seamless pipe[71-73] (by Metal Sample Company, Inc., Munford, USA), and were 5.08 cm in diameter and 0.079 cm in thickness. The chemical composition of this steel, given in Table 2, was provided by the Metal Sample Company. Results from X-ray fluorescence (XRF) for five steel membranes show that the surfaces of the membranes are homogeneous in their composition.

4.1.3 The Electrochemical Permeation Cell

Six electrochemical permeation cells were constructed. A schematic of the cell used in this study is depicted in Figure 1. The cell consists of two compartments made of Teflon and separated by the hydrogen permeation test specimen, the steel membrane. The larger, charging, compartment (about 2 L capacity) contains the test solution, which is continuously stirred by a magnetic stirrer and which charges the steel membrane with hydrogen atoms produced by H_2S corrosion reactions. To ensure a water-tight seal, Viton O-rings were used on the two sides of the steel membrane, leaving an area of 11.3 cm^2 of the membrane exposed to the solution. As shown in Figure 1 Viton O-rings are used in other parts of our cell. To remove gas bubbles that may be trapped in the hole

TABLE 2

The Chemical Composition of the Steel Membranes Used in this Study.

Steel	Grade	Concentration (wt %)								
		C	Cr	Cu	Mn	Mo	Ni	P	S	Si
A106	B	0.24	0.19	0.18	0.82	0.04	0.14	0.017	0.02	0.25

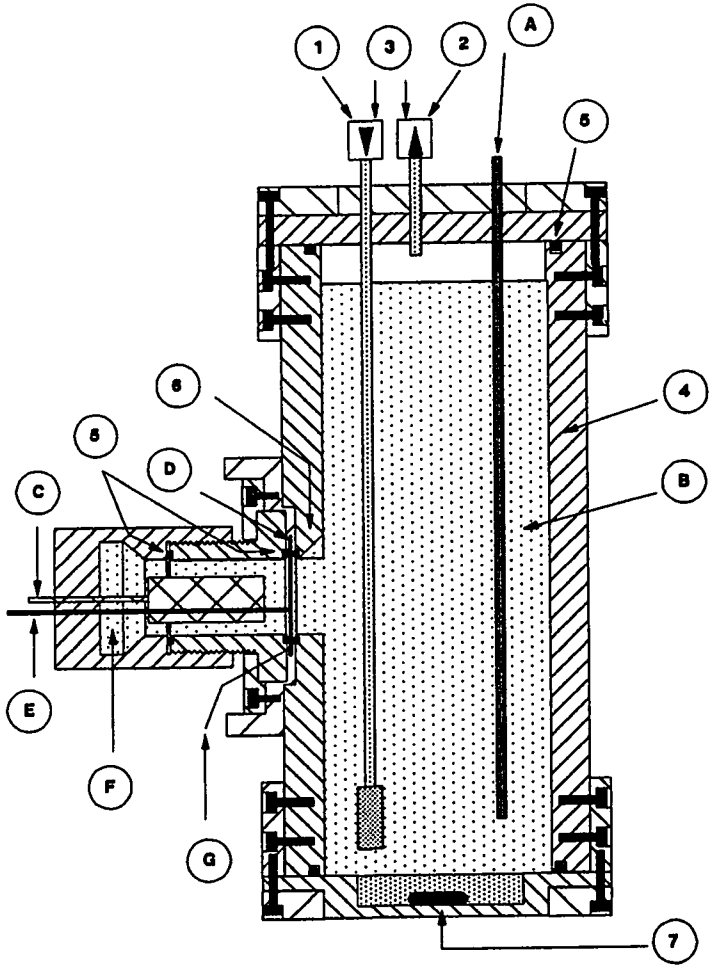

LEGEND

- (A) : Temperature Probe
- (B) : Distilled H2O + H2S + Inhibitor
- (C) : Pt Counter Electrode
- (D) : Steel Membrane
- (E) : Pt Refrence Electrode
- (F) : 0.2N NaOH Solution
- (G) : Working Electrode Connection
- (1) : Gas Inlet
- (2) : Gas Outlet
- (3) : Check Valve
- (4) : Teflon Body
- (5) : O-Ring
- (6) : Groove for Bubble Release
- (7) : Teflon Coated Stir Bar

FIGURE 1. A SCHEMATIC OF THE ELECTROCHEMICAL PERMEATION CELL.

between the steel membrane and the charging side, a groove was made as shown in Figure 1. To seal the charging side from the top and the bottom, Teflon sheets and Viton O-rings were used. The smaller, permeation, compartment contains a solution of 0.2 M NaOH, a counter electrode, and a reference electrode. The sodium hydroxide used to prepare the solutions is an AR Analytical Reagent chemical. All of the gas inlet and outlet tubes and fittings are made of Teflon.

4.1.4 The Counter Electrode

The counter electrode is a cylindrical mesh of bright platinum and is connected with a platinum rod (Alfa, Johnson Matthey Electronics, Ward Hill, USA). It is 5 cm long and 2.5 cm in diameter.

4.1.5 The Reference Electrode

The reference electrode used was a platinum wire (Alfa, Johnson Matthey Electronics, Ward Hill, USA) sealed in a glass tube by epoxy (Duralco 4700) and placed 1-2 mm away from the steel membrane (anodic side). Although a zirconium frit could be used for the reference electrode luggin capillary to stand the alkaline solution, the platinum reference electrode was preferred for easier handling.

4.1.6 The Electrical Circuit

Since hydrogen atoms were introduced into the steel membrane by allowing the latter to corrode freely in the presence of H_2S, an electrical circuit was needed only for the anodic, permeation, side. A schematic of a more advanced version of a previously designed circuit[74] for the same purpose, is depicted in Figures 2 and 3. Following is a basic description of the function of only the main components (manufactured by Analog Devices, Inc., Norwood, USA).

The voltage reference, AD588, is used to provide an accurately known voltage, in this case +5 VDC and -5 VDC from pins 1 and 15, respectively; which is utilized by the digital-to-analog (DAC) converter, AD 7846, as an external voltage reference input, necessary for its operation. The DAC set the required potential, which is fed to it by a personal computer through an IEEE-488 to parallel converter interface, through pin 5, at pin 3, the non-inverting input, of the AD 549 operational amplifier, which in turn varies the potential, through modifying the amount of current flow, of the counter electrode to maintain the required potential at the reference electrode. The instrumentation amplifier, AD 624 shown in Figure 3, provides a mean of determining the amount of current passing through the counter electrode.

This current is directly proportional to the hydrogen permeation flux, by the reduction half-reaction occurring simultaneously at the counter electrode with the

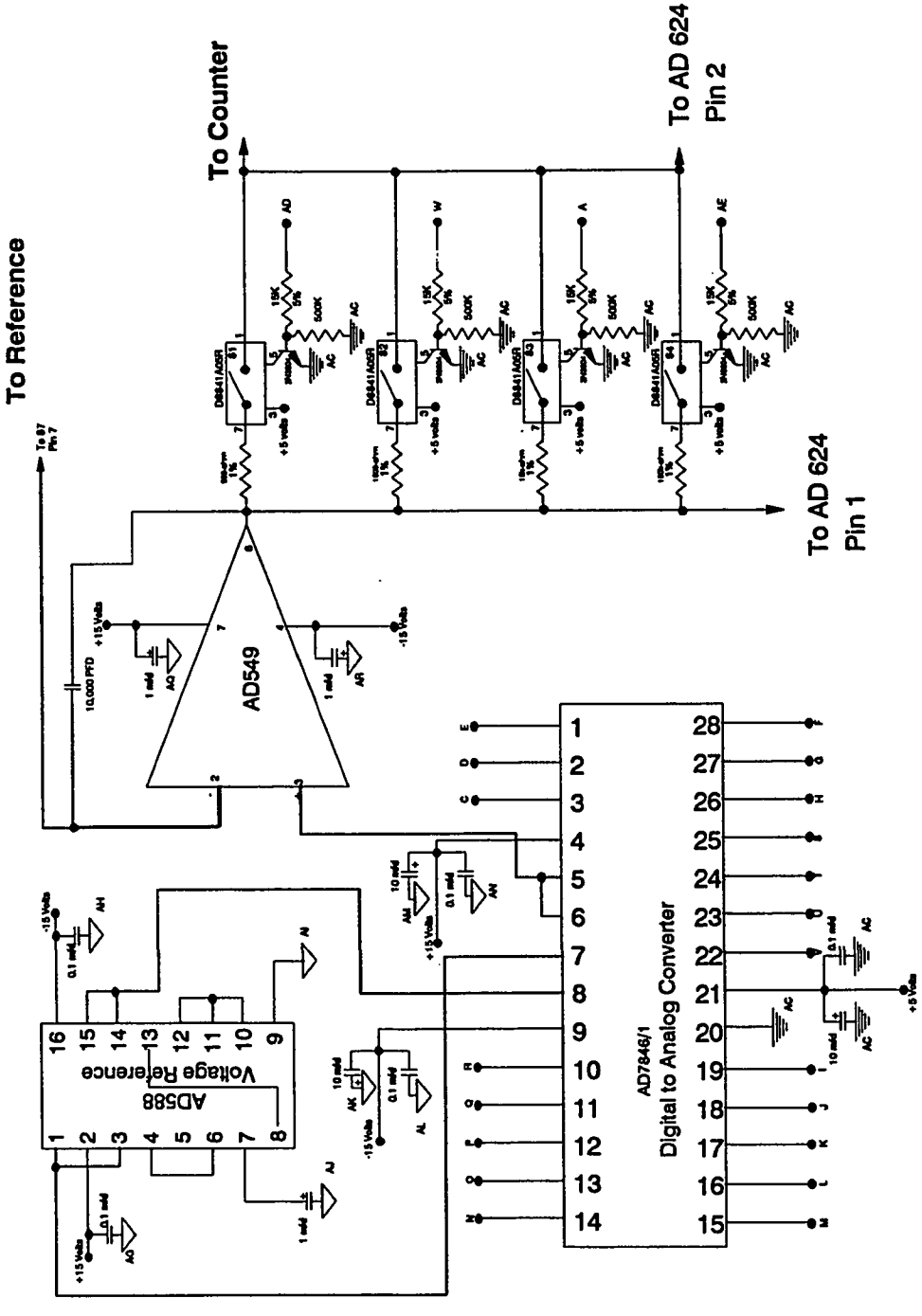

FIGURE 2. PERMEATION SIDE CIRCUITRY SCHEMATIC, PART I.

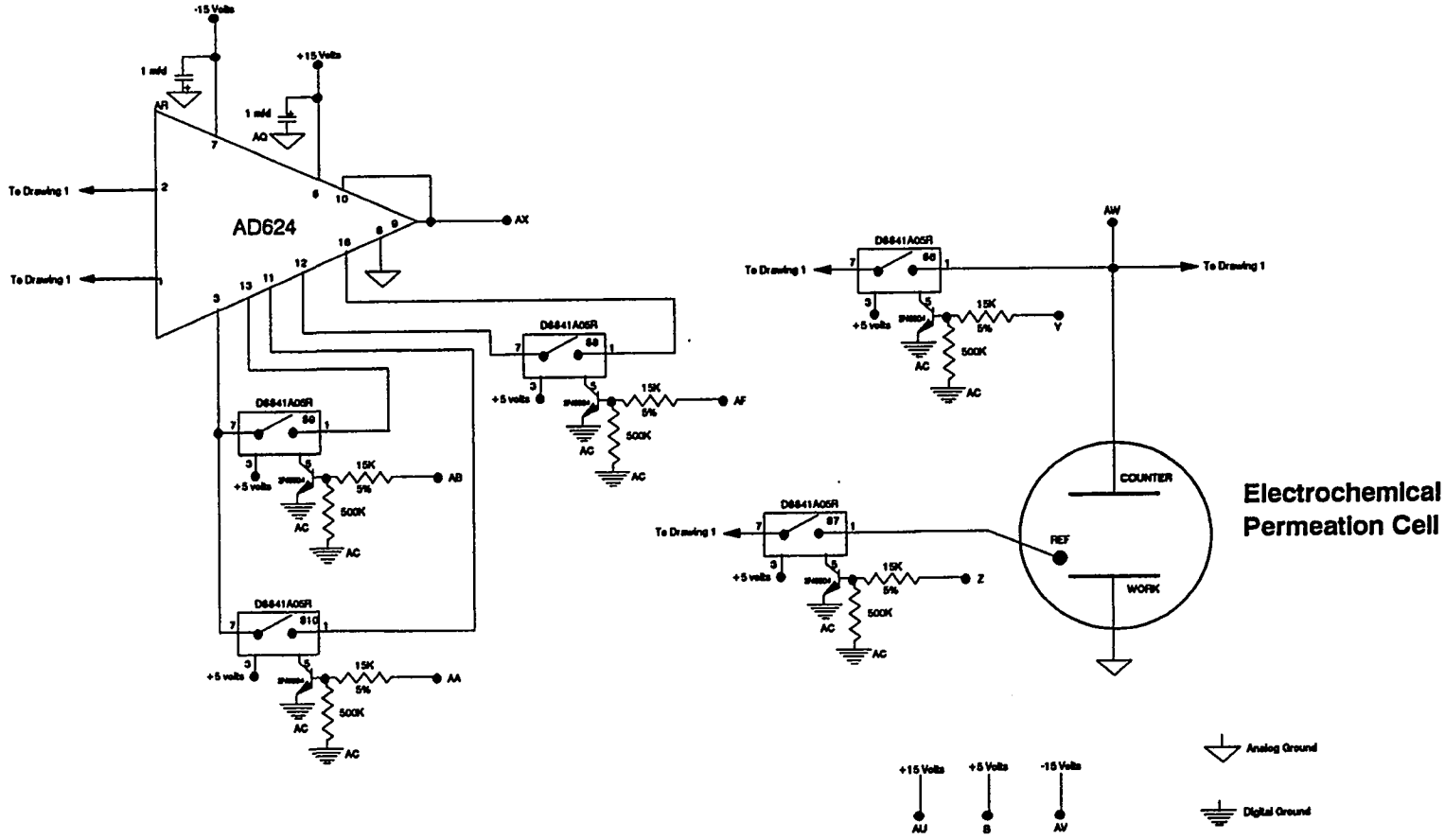

FIGURE 3. PERMEATION SIDE CIRCUITRY SCHEMATIC, PART II.

oxidation half-reaction occurring at the working electrode (the anodic surface of the steel membrane):

$$H_{ads} + OH^- \rightarrow H_2O + e^-$$

and from Fraday's laws:

$$J\left(\frac{H\text{-}atoms}{cm^2.sec}\right) = 6.24 \times 10^{12}\, i_d \left(\frac{\mu A}{cm^2}\right), \qquad [45]$$

or

$$J\left(\frac{H\text{-}moles}{cm^2.sec}\right) = 1.04 \times 10^{-11}\, i_d \left(\frac{\mu A}{cm^2}\right), \qquad [46]$$

where J and i_d are the hydrogen permeation flux and the current density, respectively.

After the electrical circuit was designed, six printed circuit boards needed to run six electrochemical permeation cells were constructed. This was accomplished by plotting the electrical circuitry so that the actual electronic components will fit into position, once the design is laid down on a copper clad board. Printouts of the actual circuit draft were made on transparencies, using a laser printer, and were ironed to a double face copper boards. The boards were, then, etched in a saturated $FeCl_3$ solution at 38°C, and the electronic components were soldered to the printed circuit boards.

4.1.7 The Complete Measurement System

A schematic of the complete electrochemical system is depicted in Figure 4, which consists of: H_2S gas cylinder (99.7% pure), N_2 gas cylinder (99.5% pure), five electronically operated flow mass controllers (Sierra Instruments, California, USA, 0-100 ml/min), five permeation cells, saturated NaOH solution for H_2S absorption, five Teflon coated 4-wires cables (Alpha Wire Corporation, New Jersey, USA), the electronic measurement system, an IEEE-488 to parallel converter interface (ICS Electronics Corporation, Model 4833, San Jose, USA), a personal computer (IBM PS/2 Model 70, 386), five digital stirrers (Cole-parmer, 04644-series), and other accessories, shown in the Figure.

4.2 Preparation of Materials

4.2.1 Preparation of the Membranes

To degrease the steel membranes, they were placed in a beaker filled with acetone and the beaker was placed in an ultrasonic vibrator (Cole-Parmer 8851 or Bransonic 220, Shelton, USA) for thirty minutes. The membranes were then rinsed with distilled water and dried with a tissue paper. A wire was soldered to the anodic side of each membrane to facilitate electric contact, using a mini-torch (Blazer, Japan) and an acid core solder (Kester Solder, Litton Systems Inc., Chicago, USA). The flux formed during

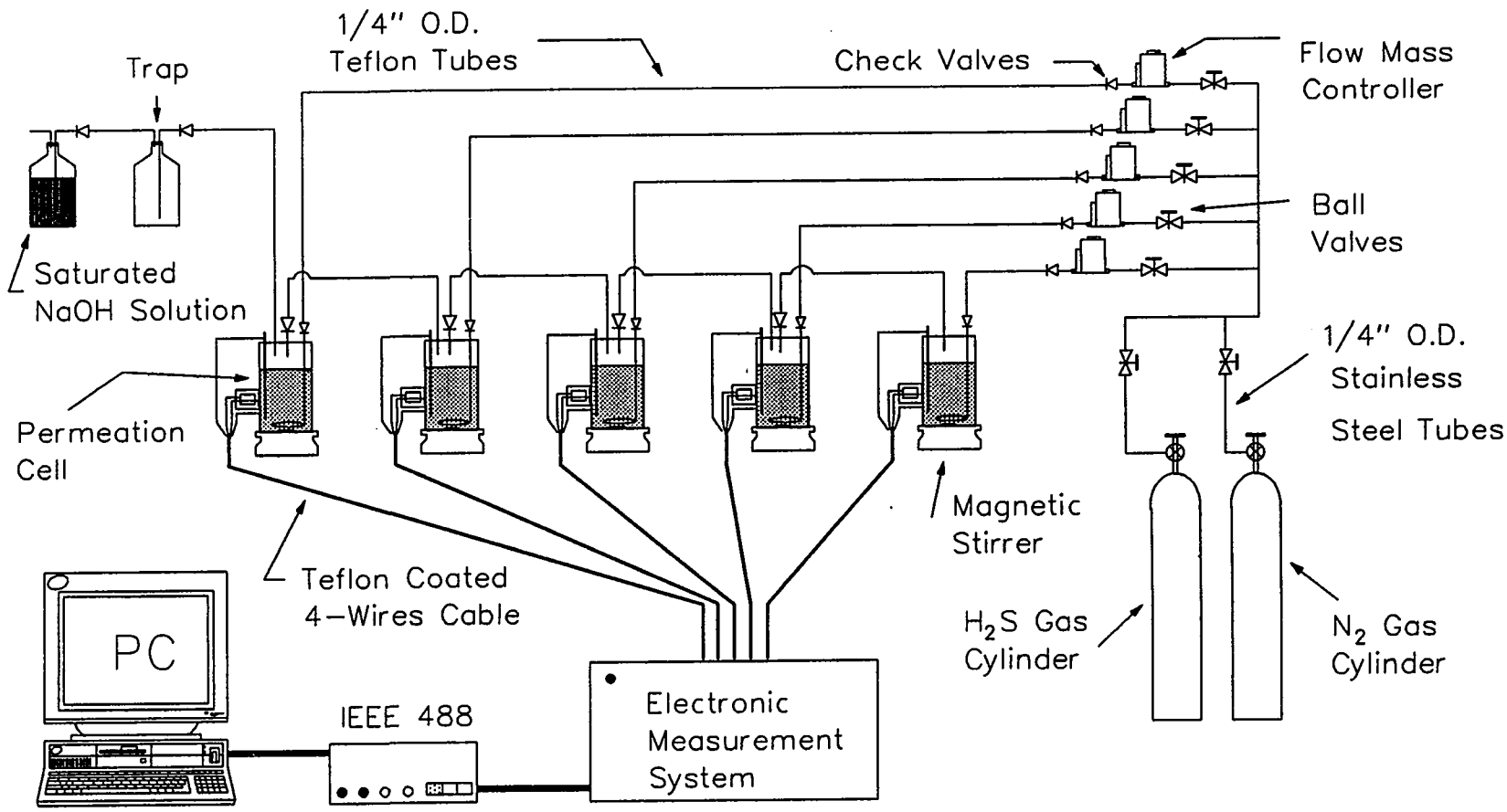

FIGURE 4. THE COMPLETE ELECTROCHEMICAL HYDROGEN PERMEATION MEASUREMENT SYSTEM.

the process of soldering was removed by isopropanol. The side of the membrane that is exposed to the corrosive environment was polished using a 600 grit abrasive paper, and the membrane was again rinsed with distilled water and dried with a tissue paper before use.

For a previously used membrane, the corrosion products were removed with steel wool, and the membrane was polished, consecutively, with abrasive papers numbers 240, 320, 400, and 600 grit (using Buehler polisher machine, Coventry, England), rinsed with distilled water, and dried with a tissue paper before it is used again.

4.2.2 Water

Distilled water was further purified using a small R.O. unit (Milli-Q Plus Water Purification System, Millipore, Molsheim, France) to remove organic and other impurities, with the final product having a resistivity of 18 MΩ.cm. This water was used for the preparation of the solutions.

4.2.3 The Preparation of the Stock Solutions

The concentration regions were chosen after consulting the literature[75] and after performing several preliminary experiments. Three stock solutions 0.015, 0.15, and 1.5 M were prepared for each of the five compounds studied. Table 3 gives the exact

TABLE 3

Concentrations of the Stock Solutions for the Five Chemicals.

Chemical	Concentration (M)		
	Stock Soln. #1	Stock Soln. #2	Stock Soln. #3
Diethanolamine	0.0156	0.156	1.56
Morpholine	0.0155	0.155	1.55
Triethanolamine	0.0155	0.155	1.55
Ethylenediamine	0.0154	0.154	1.54
Hexamethylene diamine	0.015	0.15	1.5

concentrations of the stock solutions for the five chemicals. For the high concentration of the hexamethylene diamine solutions heating was necessary to facilitate dissolution. Air-tight amber glass bottles were used to store the solutions.

4.3 The Procedure for a Permeation Experiment

The charging compartment was laid horizontally and the steel membrane was placed properly on the Viton O-ring. The permeation compartment was attached to the charging compartment and filled with a 0.2M NaOH solution. The cell was then turned vertically. The magnetic stirrer bar was placed in the charging compartment and 1500 *ml* distilled water was added to this compartment. After that, the cell was placed on the magnetic stirrer, the gas tubes were connected and the cell was completely sealed. The charging compartment was then purged with nitrogen gas. The five four-wire cables were connected to the proper cells and electrodes, and the electrochemical measurement was started by feeding the personal computer with the proper information. These include selecting the type of the experiment to be conducted (in this case "Permeation Measurement"), entering the name of the computer file where the data should be stored, entering the name of the chemical studied, specifying the total duration of the electrochemical measurement, inputting the diameter of the permeation electrode and a value for the anodic potential in the permeation side. Nitrogen gas was shut off when a stable reading was attained, followed by H_2S gas injection and simultaneously making a mark on the permeation curve.

After the hydrogen permeation current density reached a maximum steady-state value or at the end of the experiment H_2S gas flow was stopped. Sodium hydroxide pellets were then added to the charging compartment to neutralize the hydrogen sulfide-saturated solution. Finally the cell was disassembled, cleaned, rinsed with distilled water and dried with a tissue paper. During the cleaning of the cell, wearing an acid gas mask and gloves is highly recommended.

4.3.1 Selection of the Anodic Potential

Several preliminary permeation experiments were conducted to examine the maximum hydrogen permeation current density against different anodic potentials to select an appropriate hydrogen oxidation potential versus the Pt reference electrode. The results of these preliminary experiments are given and discussed in section 5.1.

4.3.2 Studying Bare Steel Membranes

Several permeation experiments were performed to study hydrogen permeation current density of bare (i.e. with no Pd electroplating on one of the surfaces) steel membranes at different anodic potentials. The results of these experiments are given and discussed in section 5.2.

4.3.3 Establishing Reproducibility

Several permeation experiments were conducted to establish reproducibility across the five cells using different steel membranes, and to establish the reproducibility of one cell using the same steel membrane several times. The results of these experiments are given and discussed in section 5.3.

4.3.4 Studying the Effect of Na_2CO_3

The sodium hydroxide solution, used in the permeation compartment, could absorb CO_2 from the atmosphere to form Na_2CO_3 which could coat the counter electrode and/or the reference electrode. In one experiment, a small amount of $NaHCO_3$ was added intentionally to examine the effect of Na_2CO_3 on the behavior of the hydrogen permeation curve. No effect was observed. The results are given and discussed in section 5.4.

4.3.5 Investigating the Effects of the Amine Inhibitors

To study the effects of the five amine inhibitors, electrochemical hydrogen permeation experiments, for each chemical at a particular concentration, were conducted in the following manner: after H_2S is injected and after hydrogen permeation current density attains a relatively stable maximum steady-state value, a specific amount of the

inhibitor solution is added using a Becton Dickinson glass syringe.

The time elapsed prior to the addition of the chemicals was approximately the same (about 650 min) in all of the experiments. Consecutive additions of the same chemical in the same cell was first examined but found to be inaccurate (see section 5.5.2, Fig. 10). The experiment was stopped when a minimum value is reached or when a total experiment duration of 36 hours had elapsed (this is due to computer memory limitations). Table 4 shows a summary of the experiments conducted for each chemical and the corresponding concentrations. As shown in Table 4, the permeation experiments for morpholine and hexamethylene diamine (HMDA) at 5×10^{-4} M were repeated to establish reproducibility.

Since air bubbles inside the syringe could not be avoided completely, air was intentionally injected into the charging compartment in one experiment to study its effect on hydrogen permeation. The results show that the presence of air does not affect the hydrogen permeation process. In another experiment, NaOH was added, producing a final concentration of 5×10^{-4} M, to study its effect on inhibiting hydrogen penetration. The effect of sodium hydroxide on inhibiting the entry of hydrogen atoms into the steel is small when compared with the effects of the amines studied (Fig. 29).

TABLE 4

Summary of the Electrochemical Hydrogen Permeation Experiments Conducted in this Study, and the Corresponding Concentrations.

Conc.(M)	DEA	MOR	TEA	EDA	HMDA
5×10^{-5}	✓	✓	✓	✓	✓
1×10^{-4}	0	0	0	✓	✓
5×10^{-4}	✓	✓✓	✓	✓	✓✓
5×10^{-3}	✓	✓	✓	✓	✓
1×10^{-2}	✓	✓	✓	0	0

✓ The experiment was done once

✓✓ The experiment was done twice

0 No experiment was done

CHAPTER 5

RESULTS & DISCUSSION

A typical hydrogen permeation curve is shown in Figure 5, for a steel membrane with a thin layer of palladium (~1000Å) electroplated on the anodic side. The anodic potential used was -200 mV versus the platinum reference electrode.

5.1 The Anodic Potential

Figure 6 shows the maximum hydrogen permeation current density versus different anodic potentials. Since the counter electrode potential shifts to more anodic values (becomes more negative and therefore the Pd layer would be dissoluted or oxidized) as the hydrogen permeation transient rises, a -200 mV anodic potential on the plateau region was selected for the whole study.

Two regions can be clearly identified in the permeation current density versus anodic potential (see Figure 6) curve. From approximately -700 to 0 mV, apparently the oxidation of hydrogen atoms is the only reaction that takes place. At anodic potentials higher than (i.e. more negative than) -700 mV other oxidation reactions such as the discharge of OH^-,

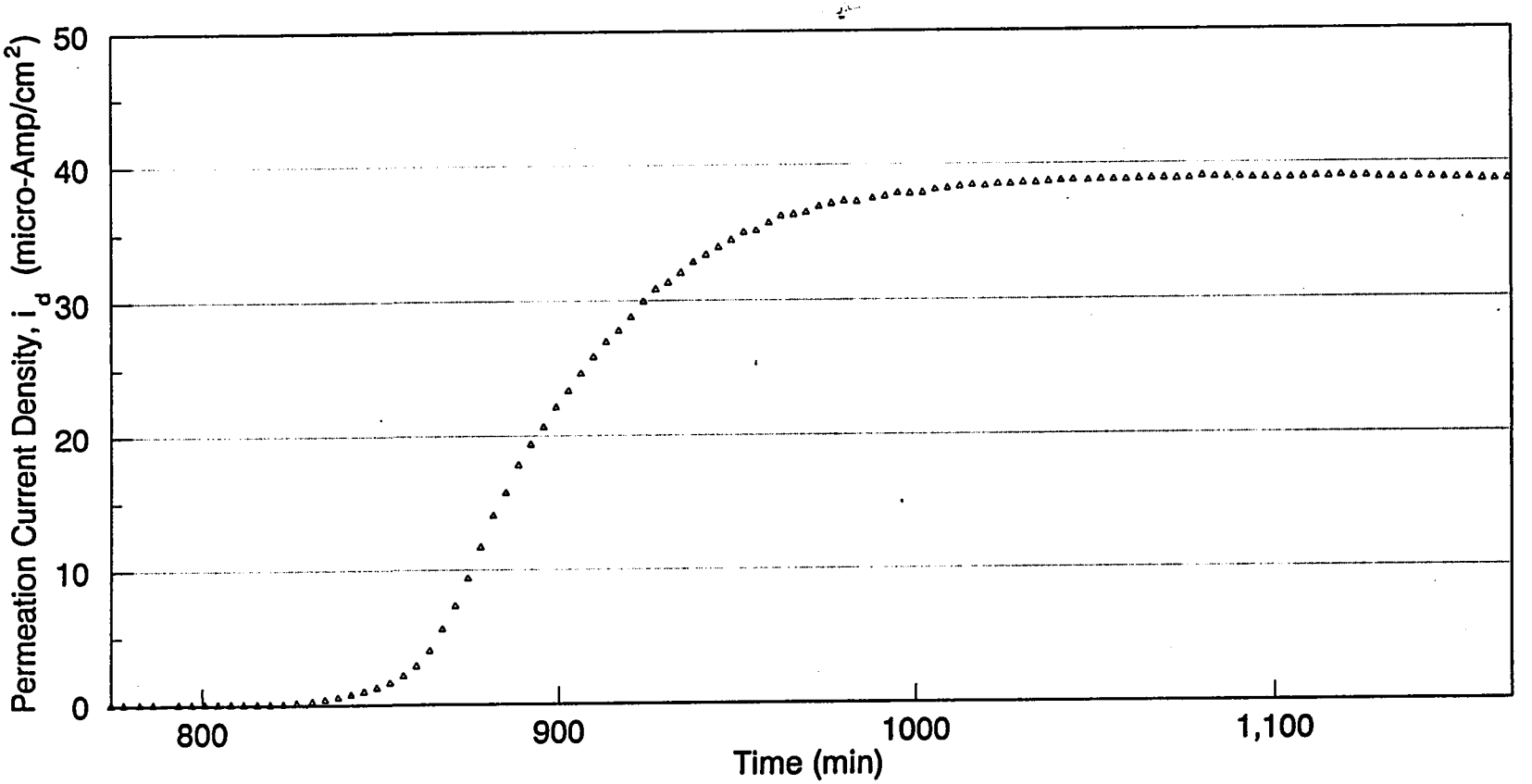

FIGURE 5. A TYPICAL HYDROGEN PERMEATION CURVE OF CURRENT DENSITY (micro-Amp/cm^2) VERSUS TIME (min), FOR A STEEL MEMBRANE (THICKNESS = 0.079 cm, AREA = 11.3 cm^2) ELECROPLATED WITH Pd (THICKNESS AROUND 1x10^{-5} cm) ON THE ANODIC SIDE. THE SOLUTION USED WAS H_2S-SATURATED DISTILLED WATER.

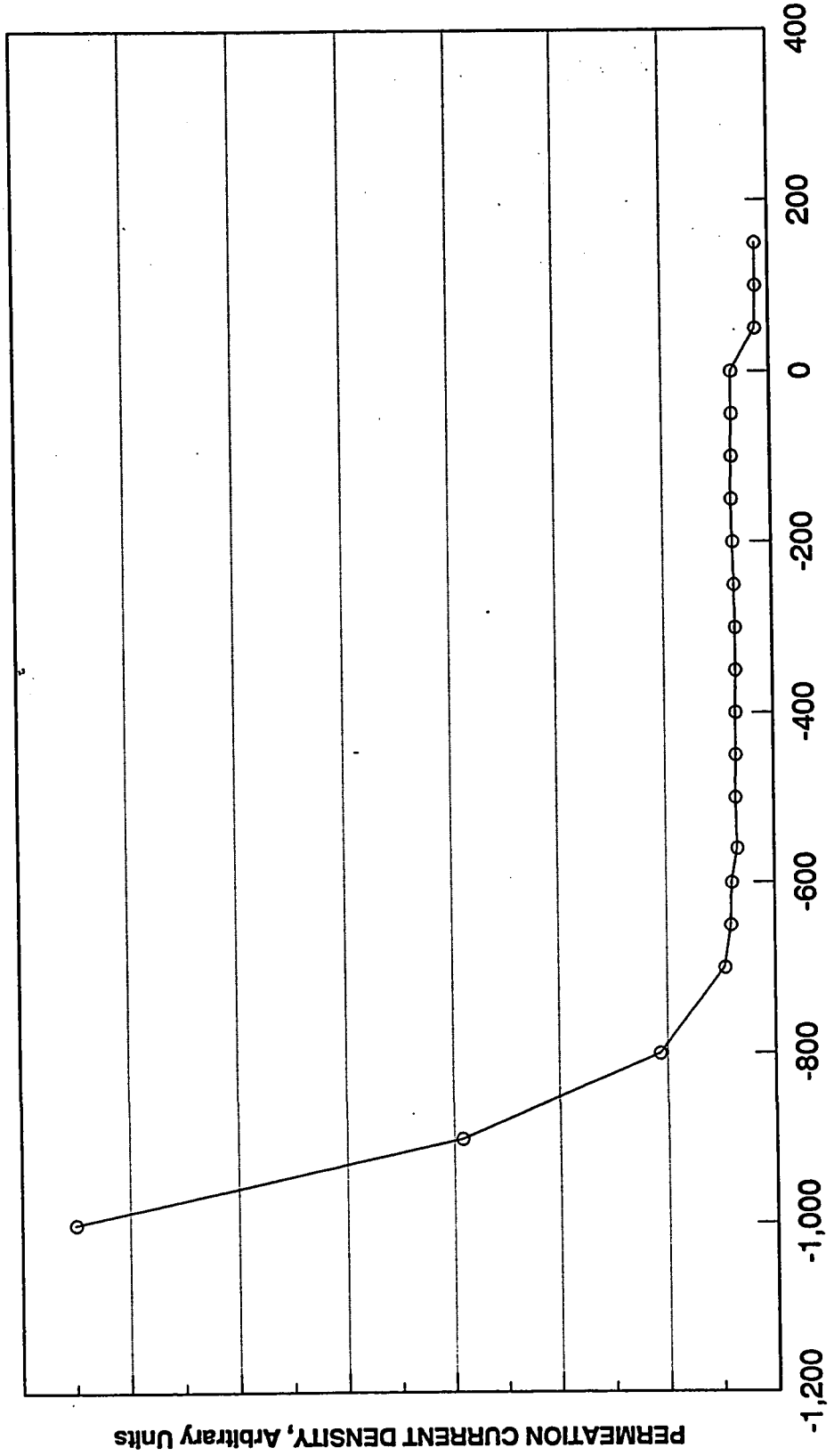

FIGURE 6. MAXIMUM HYDROGEN PERMEATION CURRENT DENSITY VERSUS ANODIC POTENTIAL.

$$4\ OH^- \rightleftarrows O_2 + 2\ H_2O + 4\ e^- \qquad [47]$$

and palladium and/or iron dissolution reactions

$$Pd \rightleftarrows Pd^{2+} + 2\ e^- \qquad [48]$$

$$Fe \rightleftarrows Fe^{2+} + 2\ e^- \qquad [49]$$

can take place.

5.2 Bare Steel Membranes

Table 5 shows the maximum hydrogen permeation current densities, at different anodic potentials, obtained for bare steel membranes, and Figure 7 displays a typical hydrogen permeation curve obtained for a bare steel membrane at an anodic potential of 0 mV versus the Pt reference electrode.

Bare steel membranes, in the presence of OH^-, will form[76] ferrous hydroxide, $Fe(OH)_2$. At sufficiently high anodic potentials $Fe(OH)_2$ is converted to iron oxide, which passivates[22] the anodic side of the steel membrane. Iron oxides are known to substantially reduce[77,78] hydrogen permeation. The relatively low maximum hydrogen permeation current densities obtained for bare steel membranes (see Table 5 and Fig. 7)

TABLE 5

Maximum Hydrogen Permeation Current Densities, $i_{d,max}$ ($\mu A/cm^2$), Obtained for Bare Steel Membranes at Different Anodic Potentials (mV) Versus the Pt Reference Electrode.

Anodic Potential (mV)	0	-50	-100	-150	-200
$i_{d,max}$ ($\mu A/cm^2$)	10.1	11.8	-	12.4	12.9

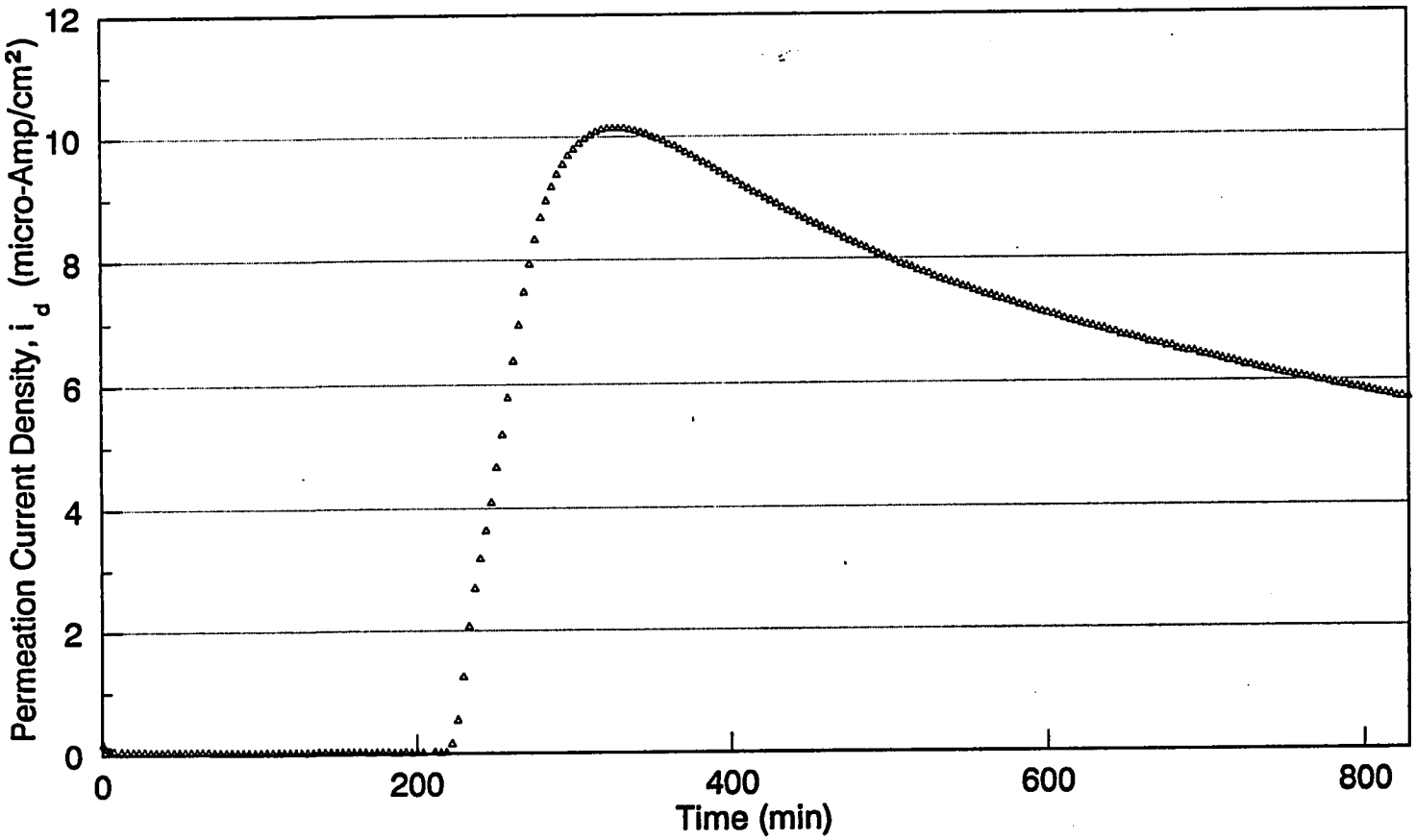

FIGURE 7. A TYPICAL HYDROGEN PERMEATION CURVE FOR A BARE STEEL MEMBRANE OBTAINED AT AN ANODIC POTENTIAL OF 0 mV VS. Pt REFERENCE ELECTRODE. THE SOLUTION USED WAS AN H_2S-SATURATED DISTILLED WATER.

are attributed to the formation of iron oxide. To avoid passivation of the anodic sides of the steel membranes a thin palladium layer was electroplated on them. Moreover, palladium has a much higher solubility for hydrogen than iron,[63] and thereby reduces the probability of the recombination of the hydrogen atoms on the exit side.

5.3 Reproducibility

Table 6 shows the maximum hydrogen permeation current densities obtained for five different steel membranes which were placed in five different permeation cells. Table 7, on the other hand, shows the maximum hydrogen permeation current densities obtained for the same membrane, which was cleaned and polished before each run, in one of the permeation cells.

In Table 6, the maximum hydrogen permeation current densities obtained for the membranes used in cells number 2, 3, and 4 were very comparable (average $i_{d,max}$ = 39.9$\pm$1.1 μA/cm^2). For the membranes used in cells 5 and 6, blistering, which was more severe for the membrane used in cell 6, was visually observed. Blistering indicates the presence of trapping sites, e.g. voids and microvoids associated with silicon impurities in the iron lattice.[18] Blisters lower $i_{d,max}$ by reducing the available diffusion paths[13] and the hydrogen atom activity in the steel lattice. The $i_{d,max}$ values for the membranes in cells 5 and 6 were 35.3 and 28.9 μA/cm^2 respectively.

TABLE 6

Maximum Hydrogen Permeation Current Densities Obtained for Five Different Steel Membranes Placed in Five Different Permeation Cells at -200 mV Versus Pt Reference Electrode.

Cell No.	2	3	4	5	6
$i_{d,max}$ ($\mu A/cm^2$)	39.6	38.9	41.1	35.3	28.9

TABLE 7

Maximum Hydrogen Permeation Current Densities Obtained for the Same Membrane Placed in One of the Permeation Cells at -200 mV Versus Pt Reference Electrode.

Trial No.	1	2	3	4	5
$i_{d,max}$ ($\mu A/cm^2$)	38.0	55.0	45.4	46.2	48.8

When a single membrane was used to examine reproducibility (Table 7), manual polishing prior to the first experiment failed to completely remove the iron sulfide film. The incomplete removal of iron sulfide is probably the cause of the low $i_{d,max}$ value of 38.0 $\mu A/cm^2$ that was obtained. Mechanical polishing prior to the second experiment resulted in a high value of 55.0 $\mu A/cm^2$ for $i_{d,max}$. Smaller $i_{d,max}$ values from trials number 3, 4, and 5 (average $i_{d,max} = 46.8 \pm 1.8$ $\mu A/cm^2$) are probably due to the partial formation of microcracks.[13]

5.4 The Effect of Na_2CO_3

For the membrane tested for reproducibility (see Table 7), an additional experiment carried out in the same cell gave a value of 45.6 $\mu A/cm^2$ for $i_{d,max}$ upon addition of $NaHCO_3$ to the hydroxide solution in the anodic compartment. This demonstrates that Na_2CO_3 has no observable effect on the measurement of the hydrogen permeation flux.

5.5 The Amine Inhibitors

5.5.1 Hydrogen Permeation Curves in the Absence of an Inhibitor

The shapes of the hydrogen permeation curves obtained at this stage deviated slightly from the shape depicted in Figure 5. The general shape of typical hydrogen

permeation curves in the absence of an inhibitor is shown in Figures 8 and 9. This general shape may be explained by the following three processes.

(i) Several workers[13,15,79-81] propose that when the concentration of hydrogen atoms in the metal exceeds a certain critical value, C_{crit}, trapping sites are activated and microcracks form at the surface and inside the steel membrane. When the surface microcracks fissure the number of diffusion paths is reduced and $i_{d,max}$ is reduced. On expansion microcracks form blisters. Although blisters were visually observed in the early experiments (cf. Fig. 5) the characteristic humps observed in Figures 8 and 9 were not present. One possible explanation is that the hydrogen atom concentration in the steel membrane was close to but did not reach C_{crit} thus the hump did not appear or was not amplified. The other possibility is that trapping sites other than voids and microvoids are responsible for the formation of this characteristic hump. The increase in $i_{d,max}$ from 38.9 $\mu A/cm^2$ (see Fig. 5) to 59.0 $\mu A/cm^2$ (see Figures 8 and 9) is probably due to the increase in H_2S input pressure from 0.7 to 1.4 atm. This increase was needed to drive enough H_2S to all five cells. The increase in $i_{d,max}$ could also be attributed to the reduced thickness of the steel membrane resulting from the successive polishing.

(ii) The contribution from the different forms of the iron sulfide film. The decay transient observed in this study is not as sharp as that reported in the literature.[13,79,81] This could be attributed to an opposing process (see section

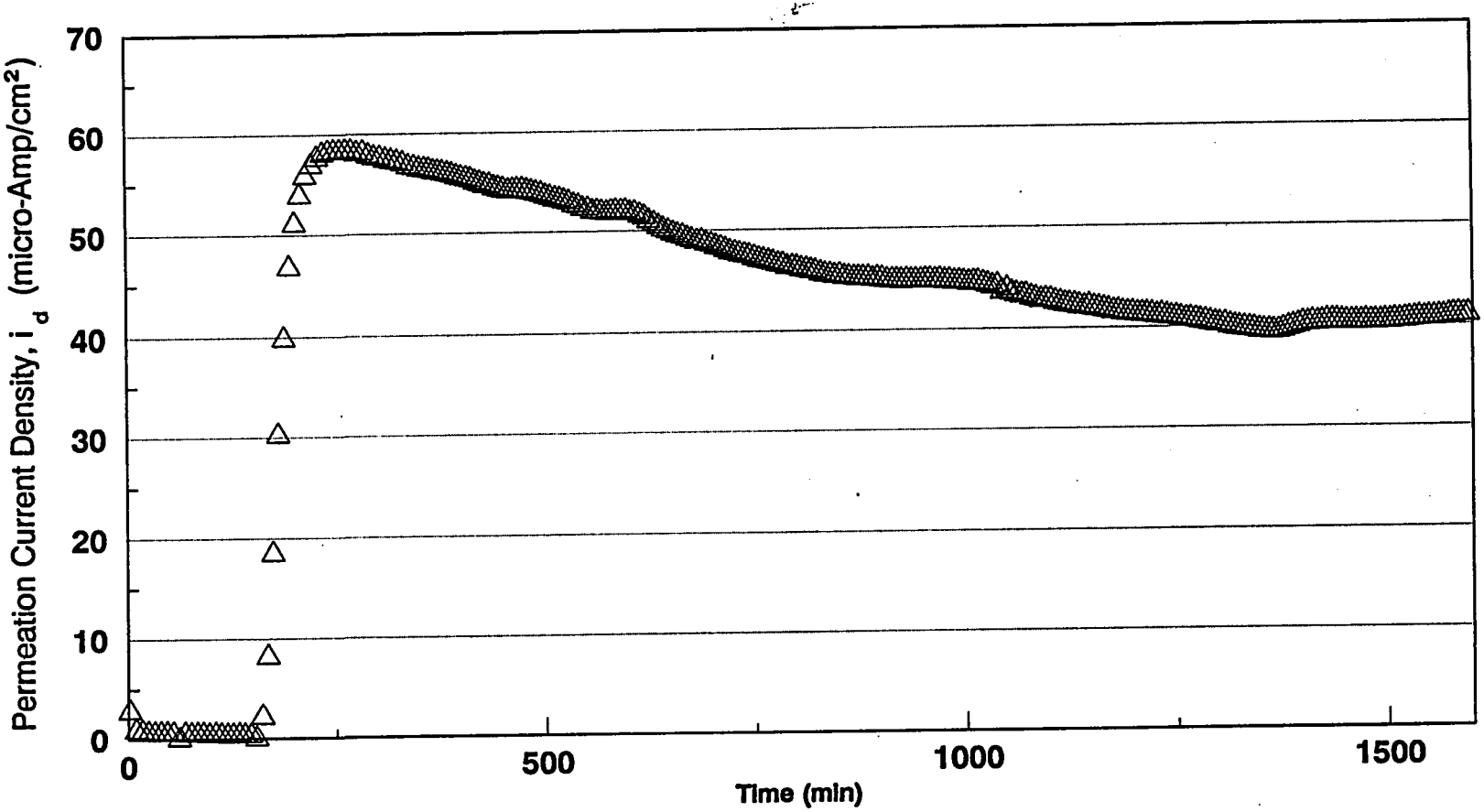

FIGURE 8. A TYPICAL HYDROGEN PERMEATION CURVE OBTAINED AT THE STAGE OF AMINE INHIBITORS EVALUATION. THE SOLUTION USED WAS AN H_2S-SATURATED DISTILLED WATER.

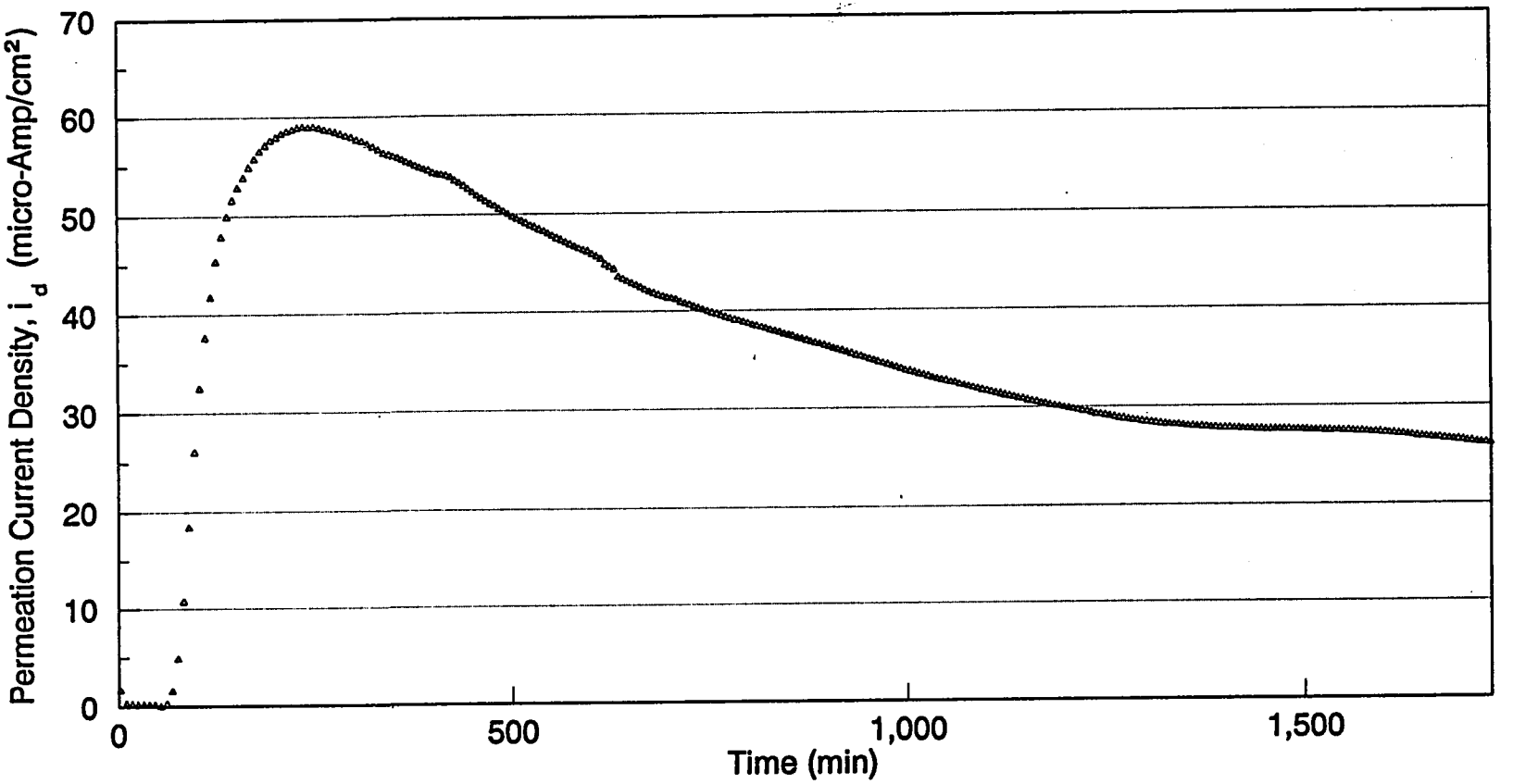

FIGURE 9. A TYPICAL HYDROGEN PERMEATION CURVE OBTAINED AT THE STAGE OF AMINE INHIBITORS EVALUATION. THE PERMEATION CURRENT DENSITY WENT TO A LOWER VALUE THAN IN FIG. 8. THE SOLUTION USED WAS AN H_2S-SATURATED DISTILLED WATER.

3.2); namely the conversion of the protective iron sulfide layer to the non-protective layer with the passage of time.[42] This conversion will result in an increase in the amount of entering hydrogen atoms.

(iii) The partial formation of a passive palladium oxide film on the anodic side at large permeation currents[56] and/or the partial dissolution of Pd and the formation of passive iron oxides. The 0.2N NaOH solution used in the anodic side of the cell during the permeation experiments was analyzed by ICP (Inductively Coupled Plasma) for Pd and Fe. Iron was present to the extent of 0.2 mg/L, while Pd was undetected; the detection limit for Pd being 0.2 mg/L. The presence of iron in the NaOH solution suggests a dissolution of the iron underneath the palladium layer. Iron will be exposed if the electroplating of palladium was not perfect or if palladium is dissoluted.

5.5.2 The Addition of an Inhibitor at Different Times During a Permeation Experiment

A typical curve showing the behavior of permeation current density versus time when consecutive additions of the same chemical into the same cell was first tried, is depicted in Figure 10. This was considered to be an unmanageable method for comparing the behavior of an inhibitor at different concentrations, and for comparing the behavior of different inhibitors at the same concentration. A clear correlation does not

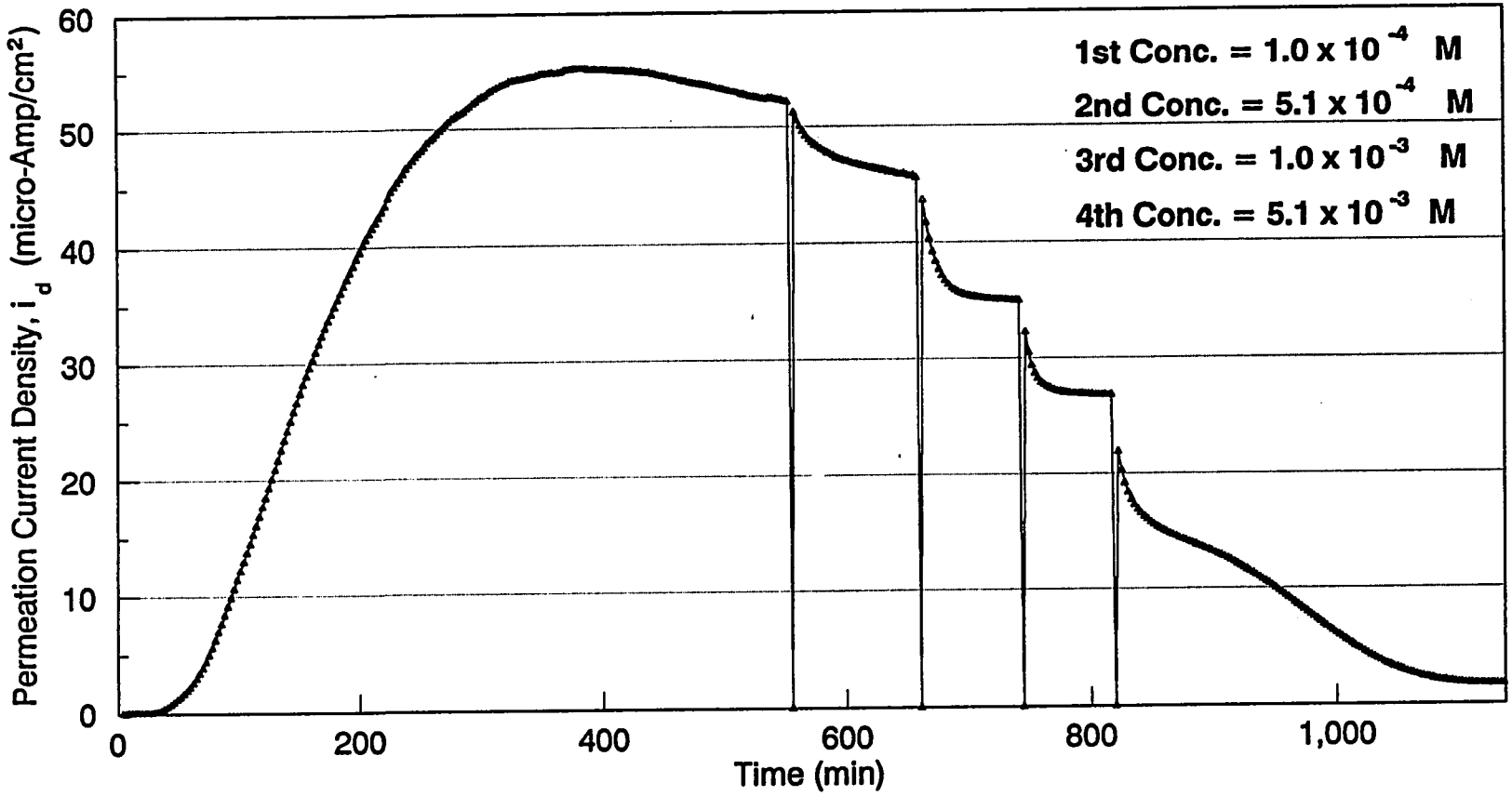

FIGURE 10. THE SHAPE OF THE PERMEATION CURVE WHEN SEVERAL ADDITIONS OF THE SAME CHEMICAL, DIETHANOLAMINE, WERE MADE AT DIFFERENT TIMES TO THE SAME CELL. THE CONCENTRATIONS GIVEN ARE OVERALL CONCENTRATIONS.

exist between the extent of inhibition after each addition and the concentration of the inhibitor. In addition, the surface of the metal membrane changes after the first addition is made and all further additions are made onto a more complex non-Langmuir surface. Moreover, the process of the interphase inhibition mechanism would have not been completed before the next addition of the inhibitor is made.

5.5.3 The One-Time Addition of the Inhibitor

Typical permeation curves with single chemical addition are shown in Figures 11 and 12, for triethanolamine at 5.2×10^{-4} M and 0.010M, respectively, and in Figure 13, for ethylenediamine at 5.1×10^{-3} M.

The following remarks summarize earlier observations. The attainment of a steady-state hydrogen permeation flux indicates: a stable hydrogen surface coverage, θ_H, at the cathodic side, the saturation of hydrogen traps present in the metal, and a stable hydrogen concentration in the metal.[3] In the presence of crack-initiation and crack-propagation processes, a hump would be observed[11] in the hydrogen permeation curve. The decay transient is only sharp initially. The slower portion of the decay transient is controlled mainly by the conversion of the iron sulfide layer (see section 3.2) from the protective form to the less protective form. A steady flux after the hump indicates that the rate at which the protective layer forms is nearly equal to the rate at which it changes to the less protective layer.

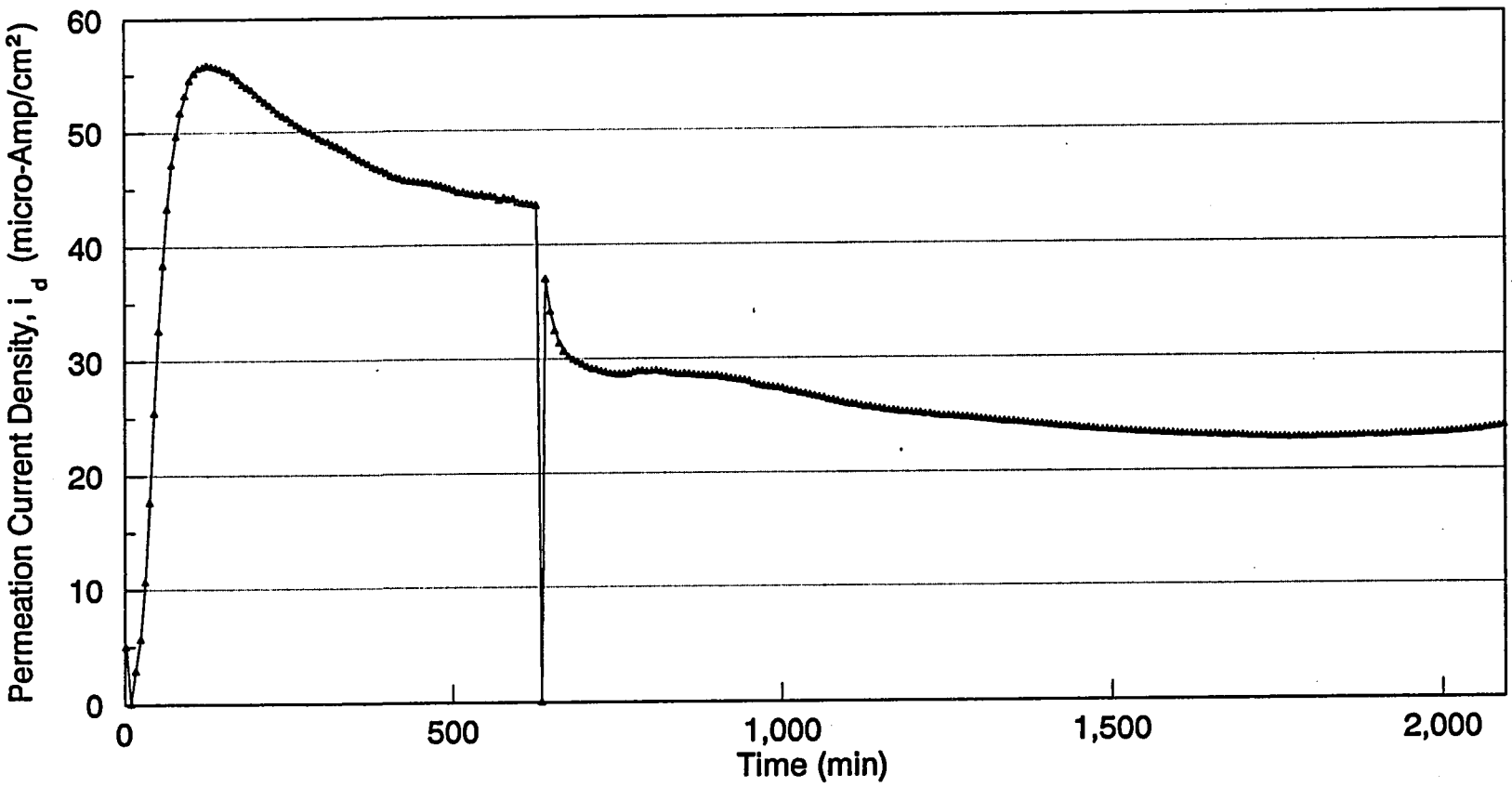

FIGURE 11. HYDROGEN PERMEATION CURVE WITH A SINGLE ADDITION OF TRIETHANOLAMINE TO GIVE A FINAL CONCENTRATION OF 5.2×10^{-4} M.

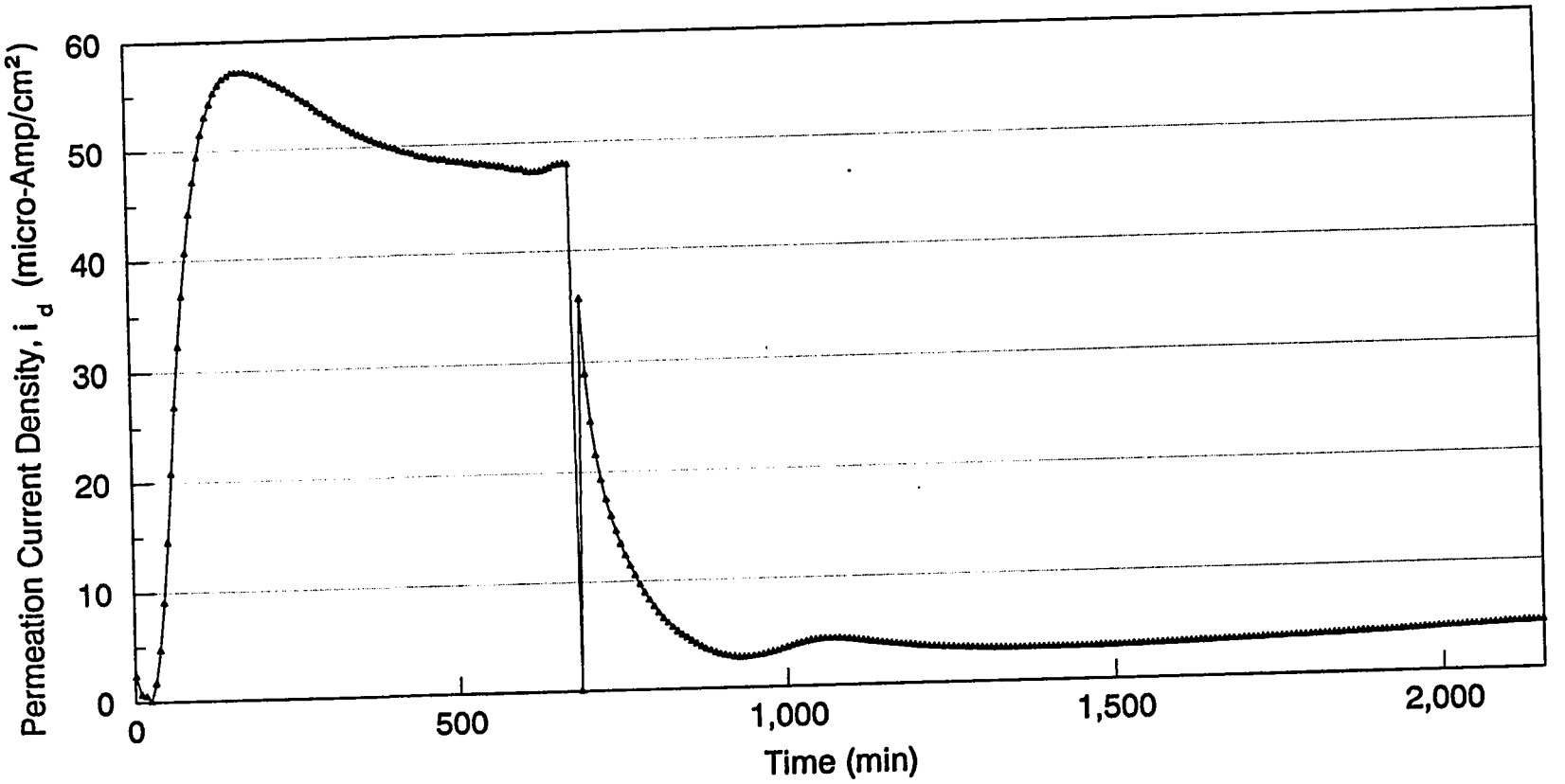

FIGURE 12. HYDROGEN PERMEATION CURVE WITH A SINGLE ADDITION OF TRIETHANOLAMINE TO GIVE A FINAL CONCENTRATION OF 0.01 M.

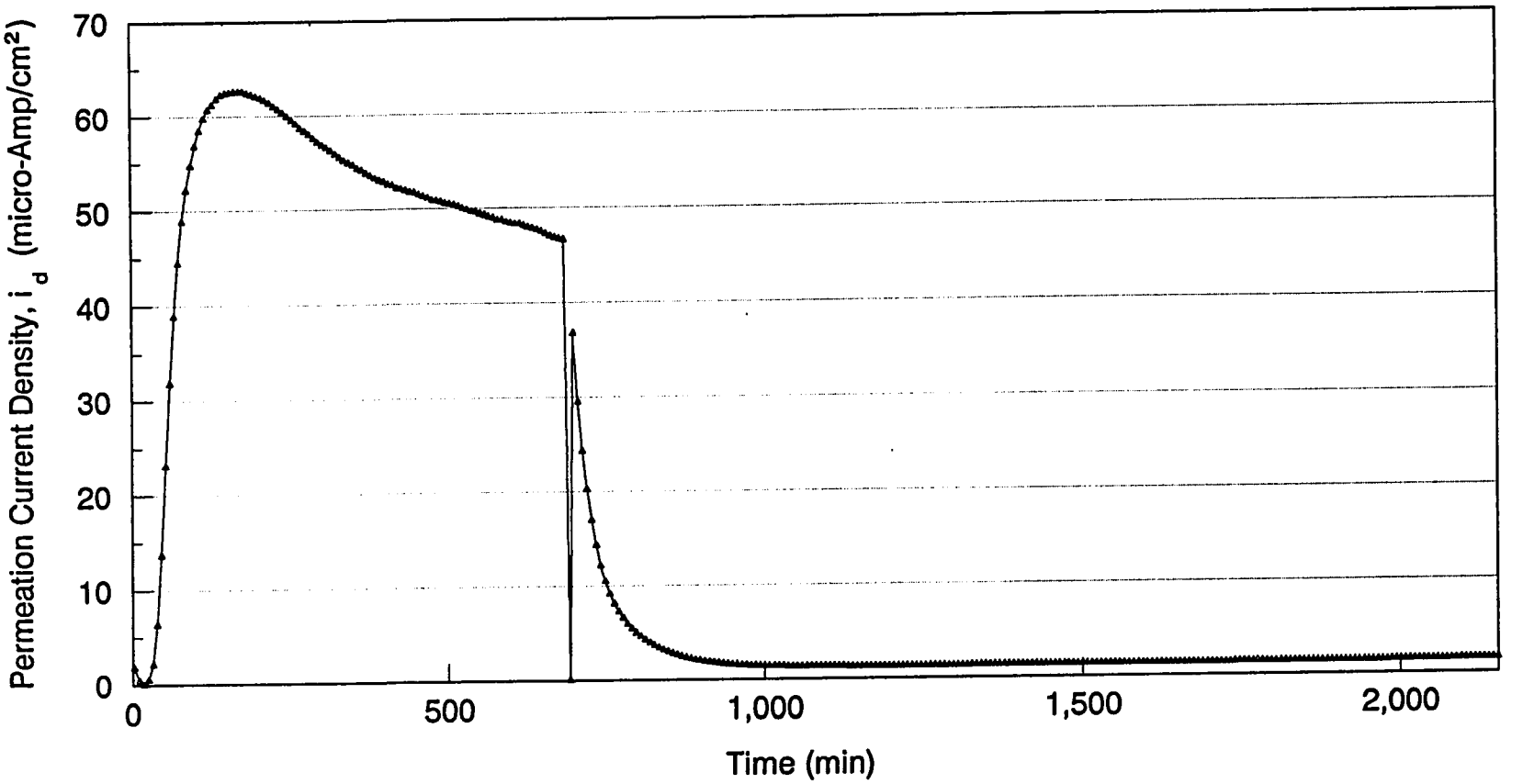

FIGURE 13. HYDROGEN PERMEATION CURVE WITH A SINGLE ADDITION OF ETHYLENEDIAMINE TO GIVE A FINAL CONCENTRATION OF 5.1 x 10^{-3} M.

The instantaneous decrease in the permeation transient after the addition of an inhibitor could be attributed to:

(i) A decrease in the diffusion coefficients of H^+ and/or HS^- in the double layer region. At this pH range (~4) H_2S and HS^- are stable,[82] thus upon the addition of the amine, an $R_3NH^+HS^-$ adduct would form, where R is a hydrogen or an alkyl group. In aqueous solutions, protons have a high mobility explainable by a chain mechanism.[83] The formation of $R_3NH^+HS^-$ adducts slows down the hydrogen atoms by disturbing their transport process. Moreover, the larger $R_3NH^+HS^-$ species are slower than HS^- since according to the Stokes-Einstein equation:[83]

$$D = \frac{kT}{f}, \quad f = 6\pi\eta\, a .$$

D is the diffusion coefficient in a solution of viscosity η, a is the effective hydrodynamic radius of the particle, and k and T are Boltzmann constant and temperature, respectively. The net effect is the reduction of θ_H and retardation of the catalytic effect of HS^-.

(ii) Interface inhibition by chemisorption according to the reaction:[33]

$$R_3NH^+ + Fe \rightleftarrows R_3NFe + H^+$$

This makes the discharge of hydrogen ions take place only at a certain distance away from the steel surface[28,46] with a higher activation energy. Furthermore,

the formation of R_3NFe prevents the formation of $Fe(HS^-)_{ads}$[34] which is a hydrogen entry promoter.

The steady and/or the slight increase in the hydrogen flux (cf. Figures 11 and 12 respectively) following the instantaneous drop could be due to the lowering of the lattice hydrogen concentration in the steel to such an extent that weakly[84] or reversibly trapped hydrogen atoms diffuse out.

The interphase inhibition mechanism is kinetically slower[29] than the interface inhibition mechanism. While the two processes could occur simultaneously, apparently, the latter is initially predominant and gives rise to a sharp decrease in current density. With the passage of time interphase inhibition becomes important resulting in a less sharp or gradual decrease. Superimposed on these processes is what we refer to as 'the secondary hydrogen atom diffusion process' which involves the diffusion of weakly or reversibly trapped hydrogen atoms.

The secondary hydrogen atom diffusion process could occur anywhere on the decay transient depending on the critical concentration, C_{crit}, of hydrogen atoms in the steel membrane, the kinetics of the interface and interphase inhibition processes, and the binding energy between trapping sites and hydrogen atoms. The hydrogen permeation curve obtained using ethylenediamine at 5.1×10^{-3} M and given in Fig. 13 shows no secondary hydrogen diffusion possibly due to the absence of weak or reversible hydrogen

trapping sites which in turn is due to the reduced thickness of the steel membrane.

Another possible cause is that following the sharp decrease (due to both interface and interphase inhibition and to the formation of $R_3NH^+HS^-$), consumption of a portion of R_3N with continuous purging with H_2S makes H_2S regain some of its activity which is then partially or completely inhibited by the formation of the interphase layer. A third possibility is that the flaking off of a thick and poorly packed interphase layer exposes the membrane surface to the corrosive medium and momentarily increases the hydrogen flux.

To compare the different permeation curves, two approaches were adopted. In the first the time of adding the chemical inhibitor to the corrosive medium was set equal to zero and the corresponding permeation current density was set equal to a 100 and this was taken as the first data point. The percent current densities at other times (up to 3 hours from t=0) were defined by

$$\% \ Current \ Density = \frac{permeation \ current \ density \ at \ t}{permeation \ current \ density \ at \ t=0} \times 100$$

and plots of percent current densities versus time were obtained. These plots will hereafter be referred to as normalized permeation curves.

In the second approach a linear least squares fit was carried out and a slope computed using the first three data points for each of the normalized permeation curves. For each inhibitor plots of the moduli of slopes versus inhibitor concentration were obtained. These will hereafter be referred to as |slope| versus concentration curves.

5.5.4 Normalized Permeation and |Slope| Versus Concentration Curves for Diethanolamine, Morpholine, and Triethanolamine

Figures 14-16, show variations in the normalized permeation curves as a function of concentration for diethanolamine, morpholine, and triethanolamine, respectively. From these figures, it is clear that as the inhibitor concentration increases inhibition becomes more effective. The figures also show that none of these compounds stimulates hydrogen entry into steel under the conditions used in this study (e.g. sour environment, room temperature, etc.).

Figures 17-20, compare the extents of hydrogen penetration inhibition of these three chemicals at the concentrations 5×10^{-5}, 5×10^{-4}, 5×10^{-3}, and 0.01 M, respectively. The following general trends are shown in these figures. As Fig. 17 shows at the low inhibitor concentration of 5×10^{-5} M the effectiveness of inhibition follows the trend TEA > MOR > DEA. At the higher inhibitor concentration of 5×10^{-4} M (Fig. 18) the effectiveness of inhibition follows the trend TEA > MOR $\approx$ DEA. At inhibitor concentrations of 5×10^{-3} and 0.01 M (Fig. 19 and 20 respectively) the three monoamines

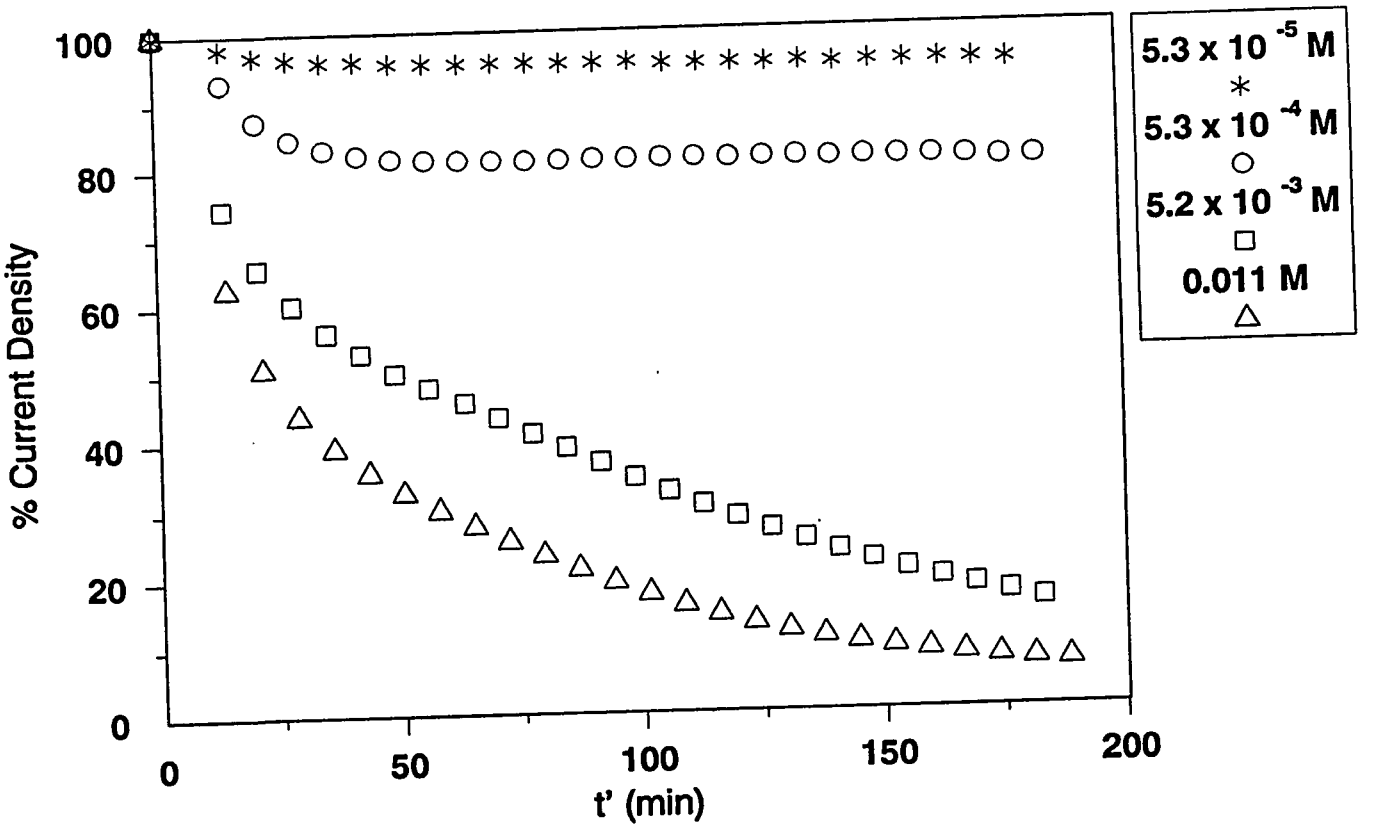

FIGURE 14. NORMALIZED PERMEATION CURVES FOR DIFFERENT CONCENTRATIONS OF DIETHANOLAMINE. THE CURRENT DENSITY AT THE INSTANT OF INHIBITOR ADDITION (t'=0) IS ASSIGNED THE VALUE 100.

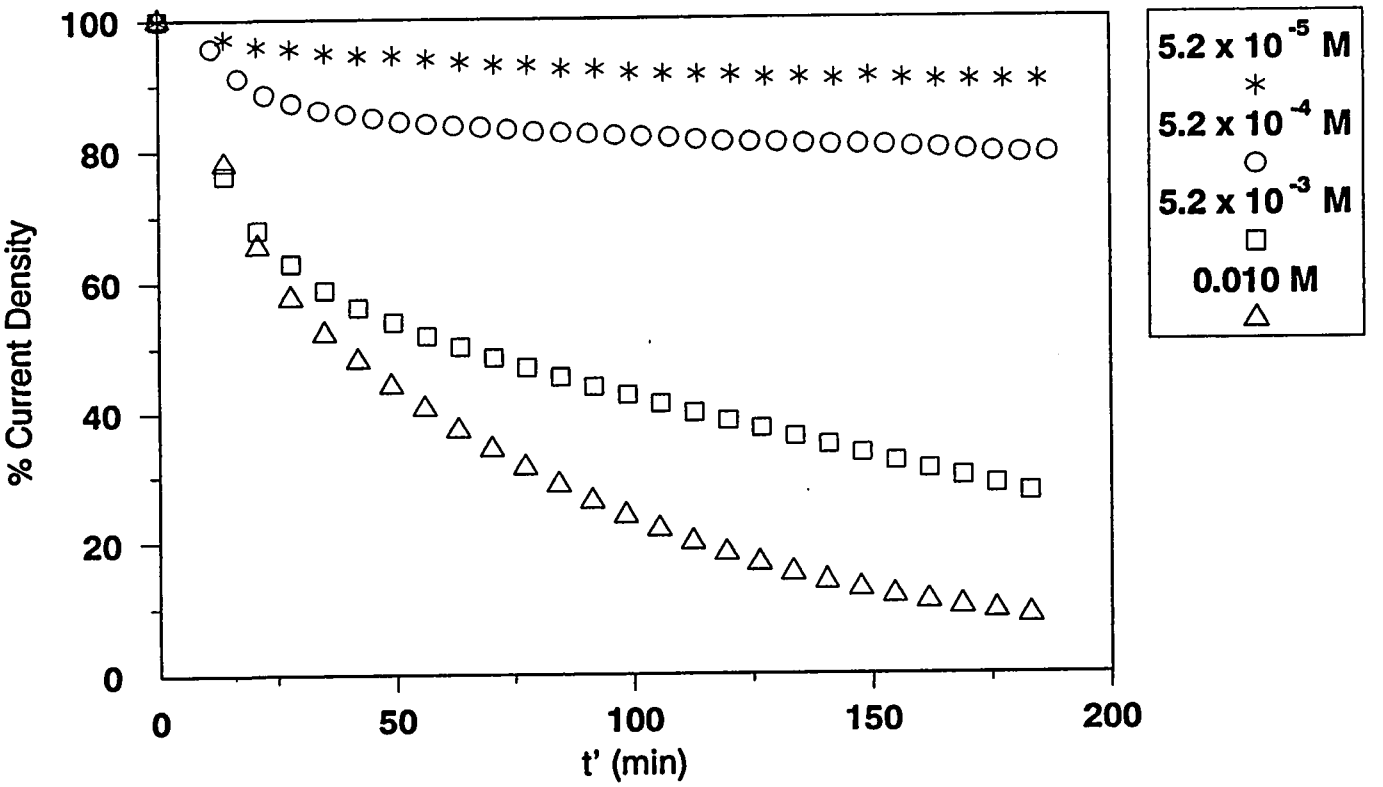

FIGURE 15. NORMALIZED PERMEATION CURVES FOR DIFFERENT CONCENTRATIONS OF MORPHOLINE. THE CURRENT DENSITY AT THE INSTANT OF INHIBITOR ADDITION (t'=0) IS ASSIGNED THE VALUE 100.

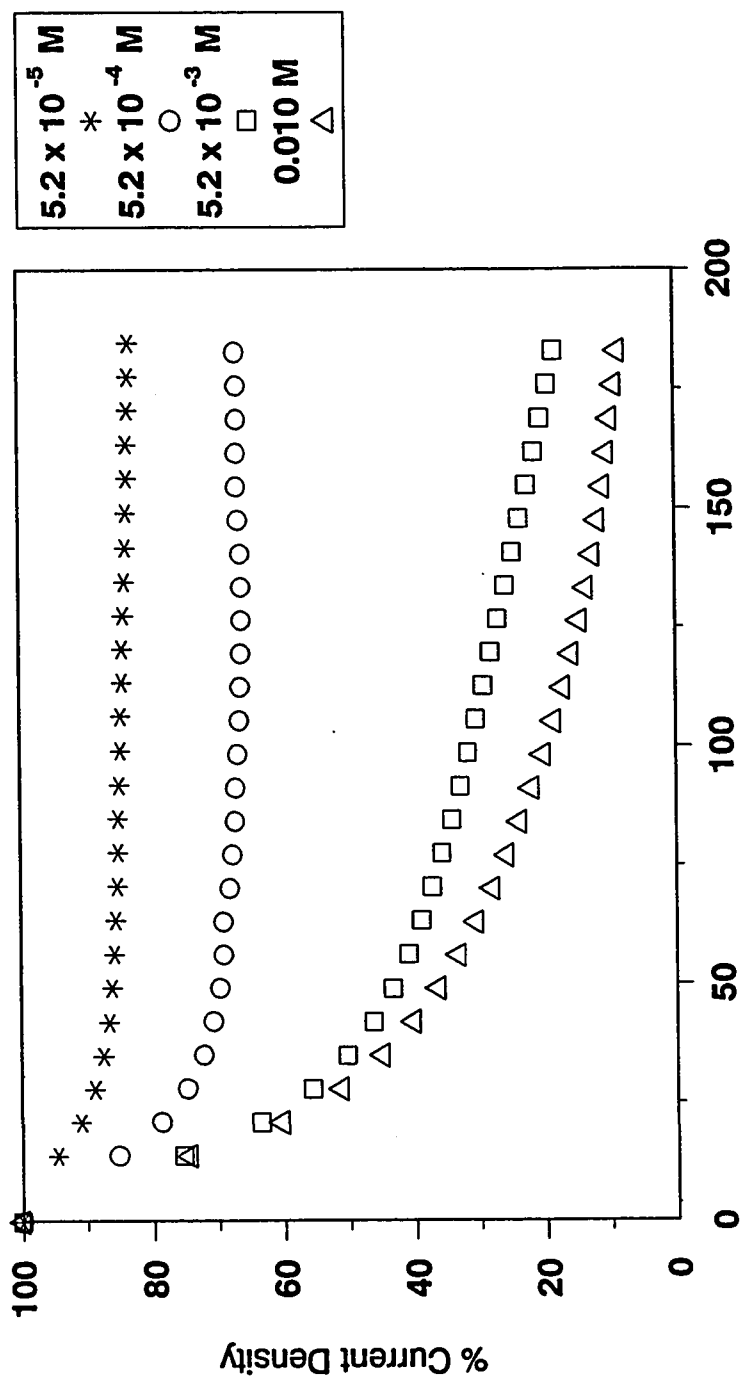

FIGURE 16. NORMALIZED PERMEATION CURVES FOR DIFFERENT CONCENTRATIONS OF TRIETHANOLAMINE. THE CURRENT DENSITY AT THE INSTANT OF INHIBITOR ADDITION (t'=0) IS ASSIGNED THE VALUE 100.

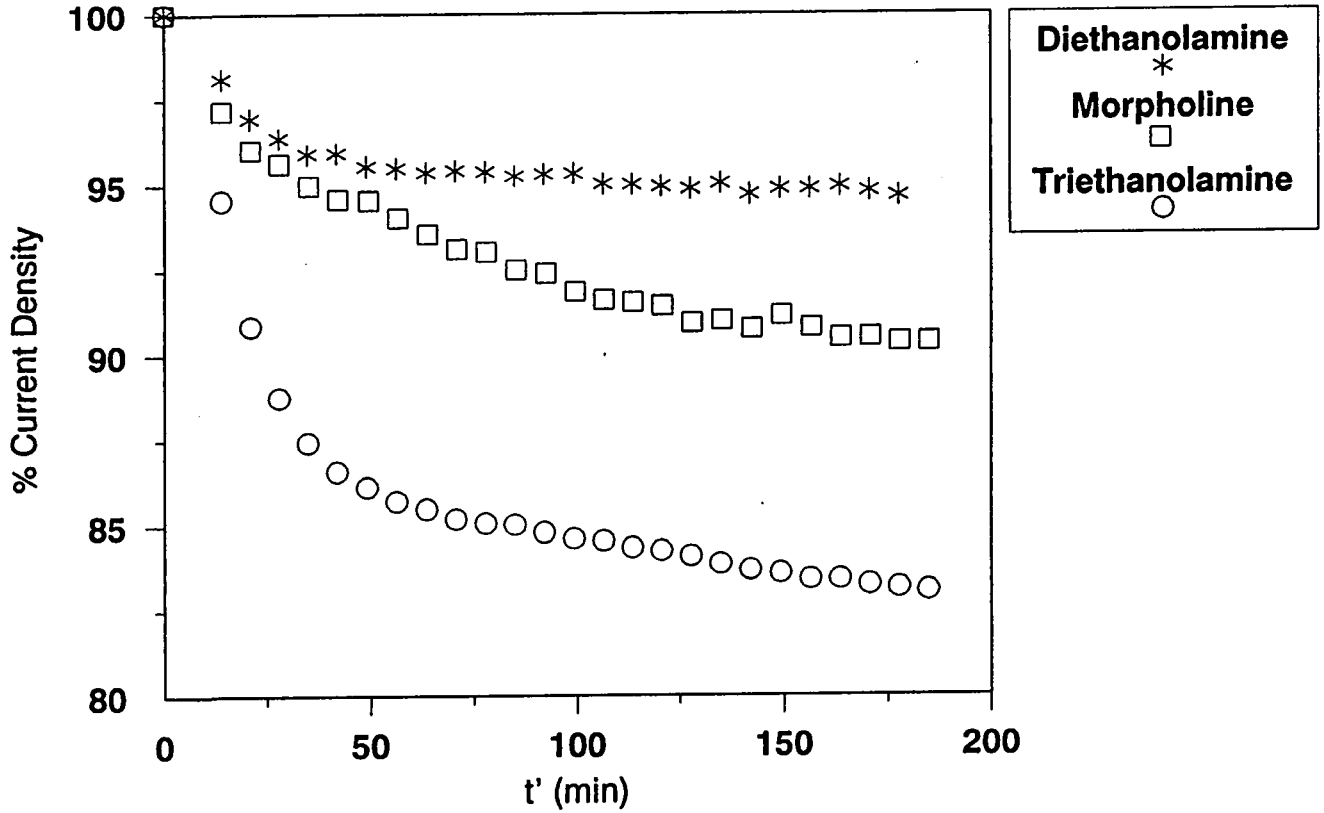

FIGURE 17. NORMALIZED PERMEATION CURVES FOR $5x10^{-5}$ M SOLUTIONS OF DIETHANOLAMINE MORPHOLINE, AND TRIETHANOLAMINE. THE CURRENT DENSITY AT THE INSTANT OF INHIBITOR ADDITION (t'= 0) IS ASSIGNED THE VALUE 100.

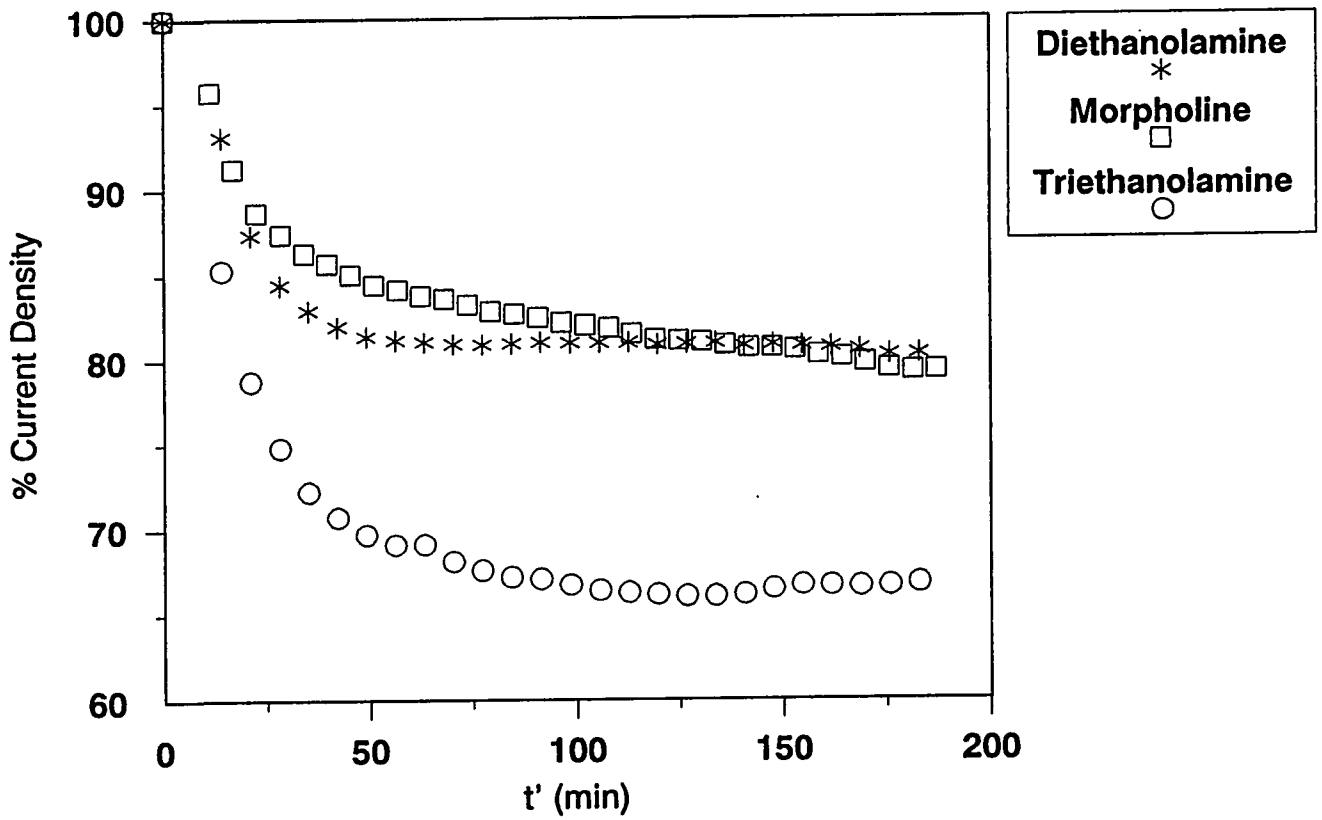

FIGURE 18. NORMALIZED PERMEATION CURVES FOR $5x10^{-4}$ M SOLUTIONS OF DIETHANOLAMINE MORPHOLINE, AND TRIETHANOLAMINE. THE CURRENT DENSITY AT THE INSTANT OF INHIBITOR ADDITION (t'= 0) IS ASSIGNED THE VALUE 100.

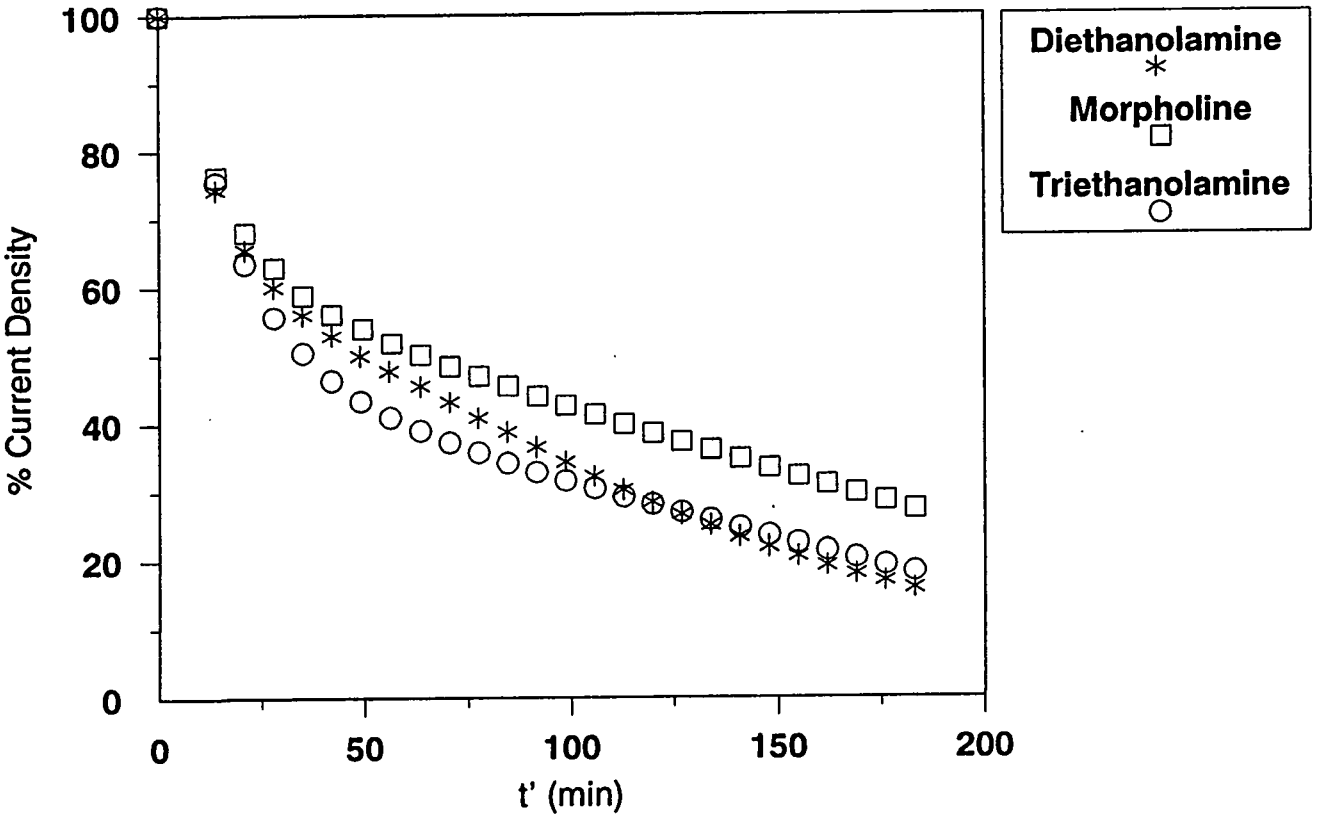

FIGURE 19. NORMALIZED PERMEATION CURVES FOR $5x10^{-3}$ M SOLUTIONS OF DIETHANOLAMINE MORPHOLINE, AND TRIETHANOLAMINE. THE CURRENT DENSITY AT THE INSTANT OF INHIBITOR ADDITION (t'= 0) IS ASSIGNED THE VALUE 100.

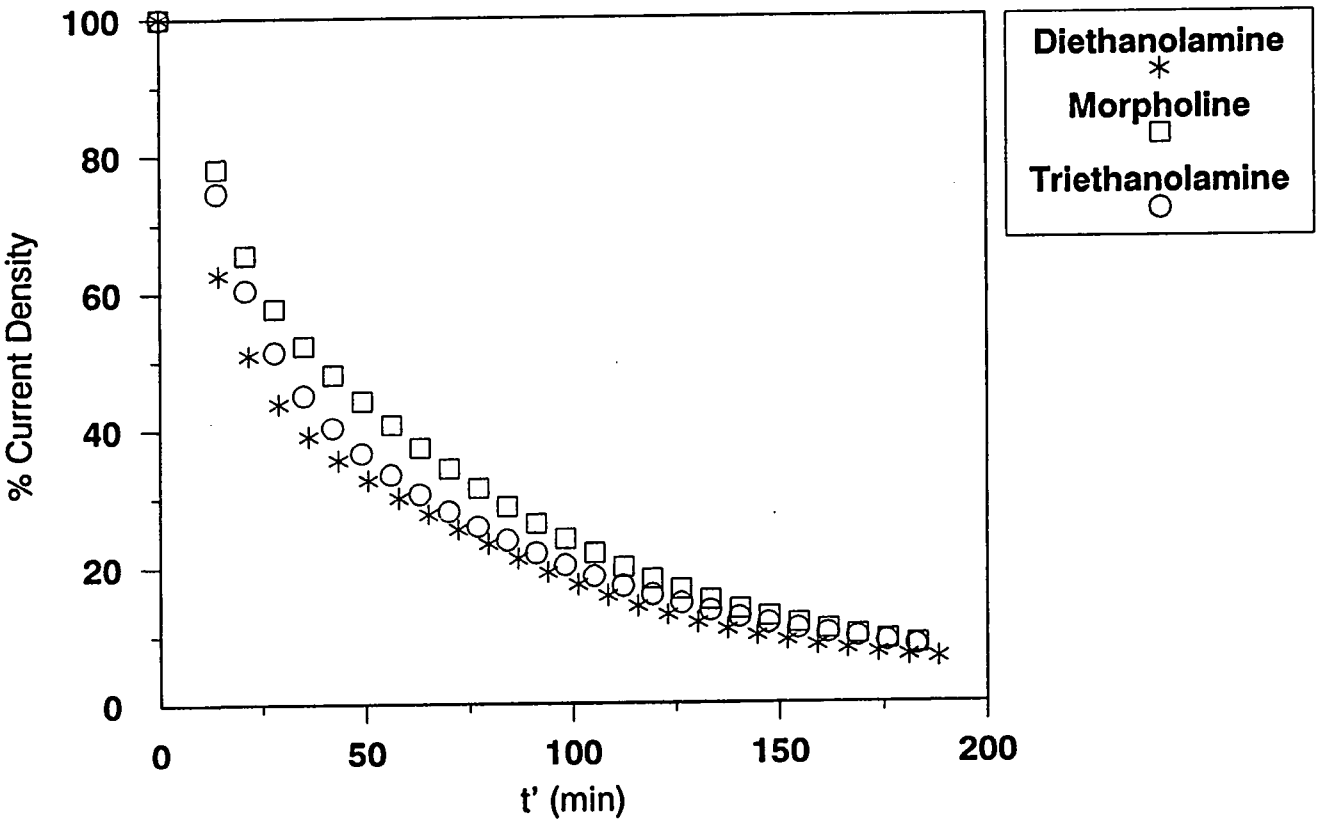

FIGURE 20. NORMALIZED PERMEATION CURVES FOR 0.01 M SOLUTIONS OF DIETHANOLAMINE MORPHOLINE, AND TRIETHANOLAMINE. THE CURRENT DENSITY AT THE INSTANT OF INHIBITOR ADDITION (t'= 0) IS ASSIGNED THE VALUE 100.

display similar inhibition effectiveness. A more careful examination of Figures 19 and 20 reveals that DEA becomes slightly more effective than MOR at 5×10^{-3} M and slightly more effective than both MOR and TEA at 0.01 M. An explanation of these observations is attempted in the following two paragraphs.

At low concentrations the reaction center, nitrogen, is apparently the determining factor in the inhibition effectiveness. In TEA, three electron donating alkyl groups are attached to the nitrogen while only two alkyl groups are attached to the nitrogen in MOR or DEA, making the electrons on the nitrogen in TEA more available than those on the nitrogen in MOR or DEA. The electron withdrawing hydroxyl groups in DEA make the electrons on its nitrogen less available than the electrons on the nitrogen of MOR. TEA possesses the additional features of a higher number of carbon atoms[75] and therefore a higher hydrophobicity and a larger projected inhibitor molecular area onto the steel surface[28], which add to its inhibition effectiveness.

At moderate coverages intramolecular hydrogen-bonding is possible in TEA and DEA but not in MOR. Such intramolecular hydrogen-bonding makes DEA and MOR nearly equal in their inhibition effectiveness at 5.0×10^{-4} M and makes DEA even slightly more effective as inhibitor at 5.0×10^{-3} M. At 0.01 M the slightly greater inhibition effectiveness of DEA relative to TEA is again attributed to greater intramolecular hydrogen-bonding in the less branched, and therefore better packed, DEA.

Figure 21 shows the |slope| versus concentration curves for diethanolamine, morpholine, and triethanolamine. The figure shows a non-linear relationship between hydrogen penetration inhibition and inhibitor concentration. The existence of a plateau for MOR and TEA shows that beyond 3.0×10^{-4} M the inhibition effectiveness reaches a 'limiting value'.

5.5.5 Normalized Permeation and |Slope| Versus Concentration Curves for Ethylenediamine and Hexamethylene Diamine

Figures 22 and 23, show variations in the normalized permeation curves as a function of concentration for ethylenediamine and hexamethylene diamine, respectively. From these figures it is clear that as the inhibitor concentration increases inhibition becomes more effective. The figures also show that none of these compounds stimulates hydrogen entry into steel under the conditions used in this study (e.g. sour environment, room temperature, etc.).

Figures 24-27, compare the extents of hydrogen penetration inhibition of these two chemicals at the concentrations 5×10^{-5}, 1×10^{-4}, 5×10^{-4}, and 5×10^{-3} M, respectively. As shown in Figure 24 HMDA is a more effective inhibitor than EDA at the lower concentration limit of 5.0×10^{-5} M. As Figure 27 shows HMDA and EDA are equally effective inhibitors at the higher concentration of 5.0×10^{-3} M. In the lower concentration limit electrons at the two nitrogens in HMDA are apparently more available

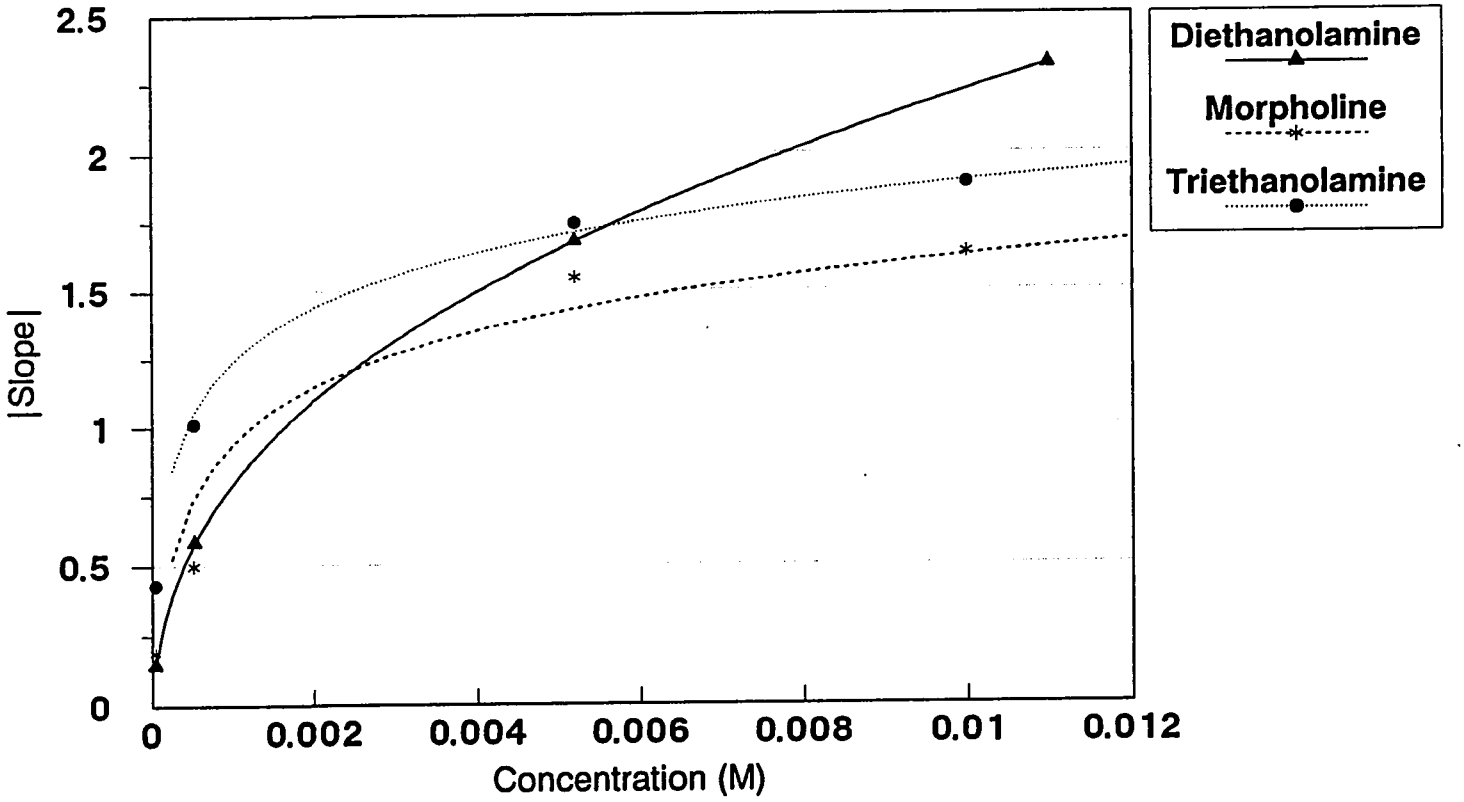

FIGURE 21. |SLOPE| VERSUS CONCENTRATION CURVES FOR DIETHANOLAIMNE, MORPHOLINE, AND TRIETHANOLAMINE. SLOPES WERE DETERMINED FROM THE FIRST THREE POINTS FOR EACH CONCENTRATION.

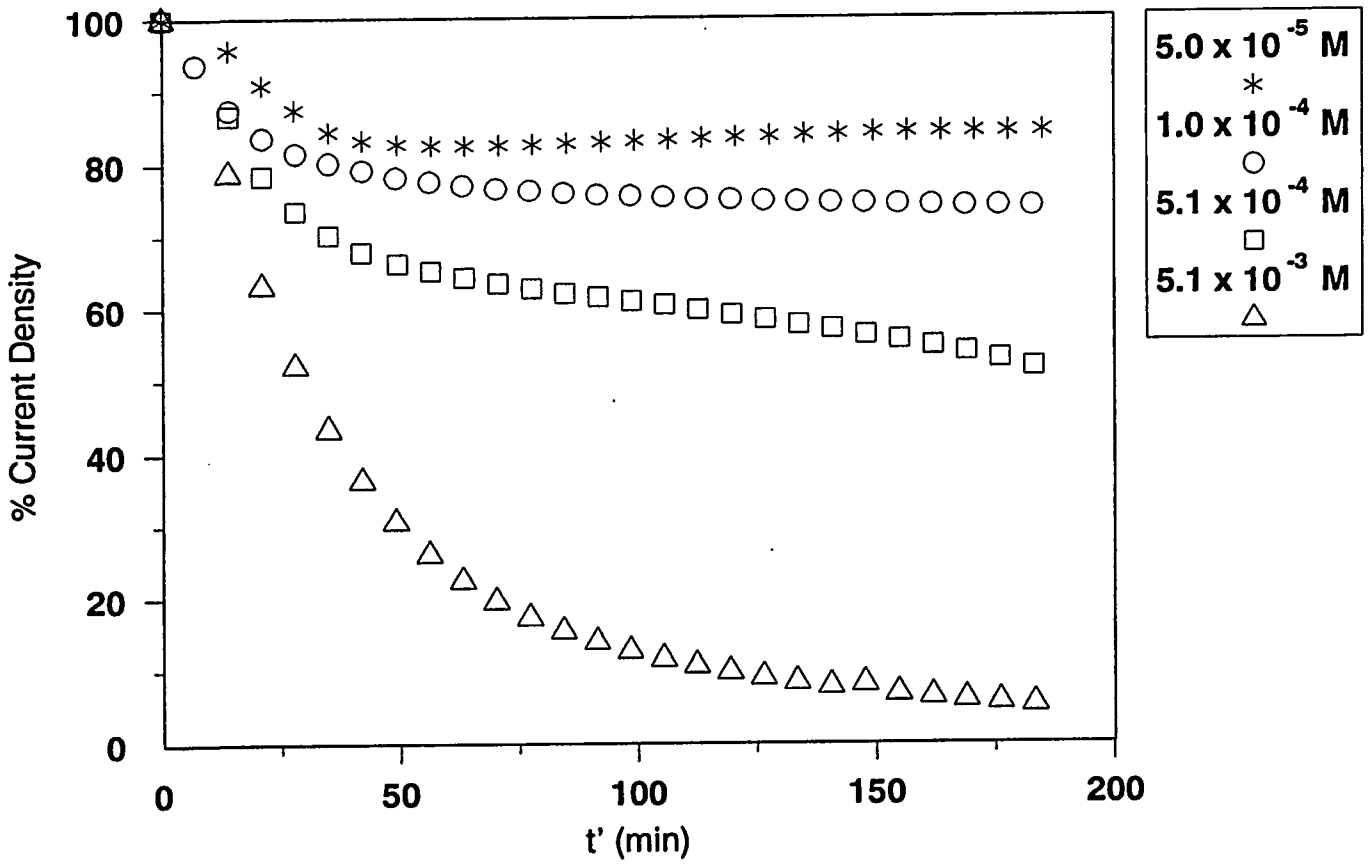

FIGURE 22. NORMALIZED PERMEATION CURVES FOR DIFFERENT CONCENTRATIONS OF ETHYLENEDIAMINE. THE CURRENT DENSITY AT THE INSTANT OF INHIBITOR ADDITION (t'=0) IS ASSIGNED THE VALUE 100.

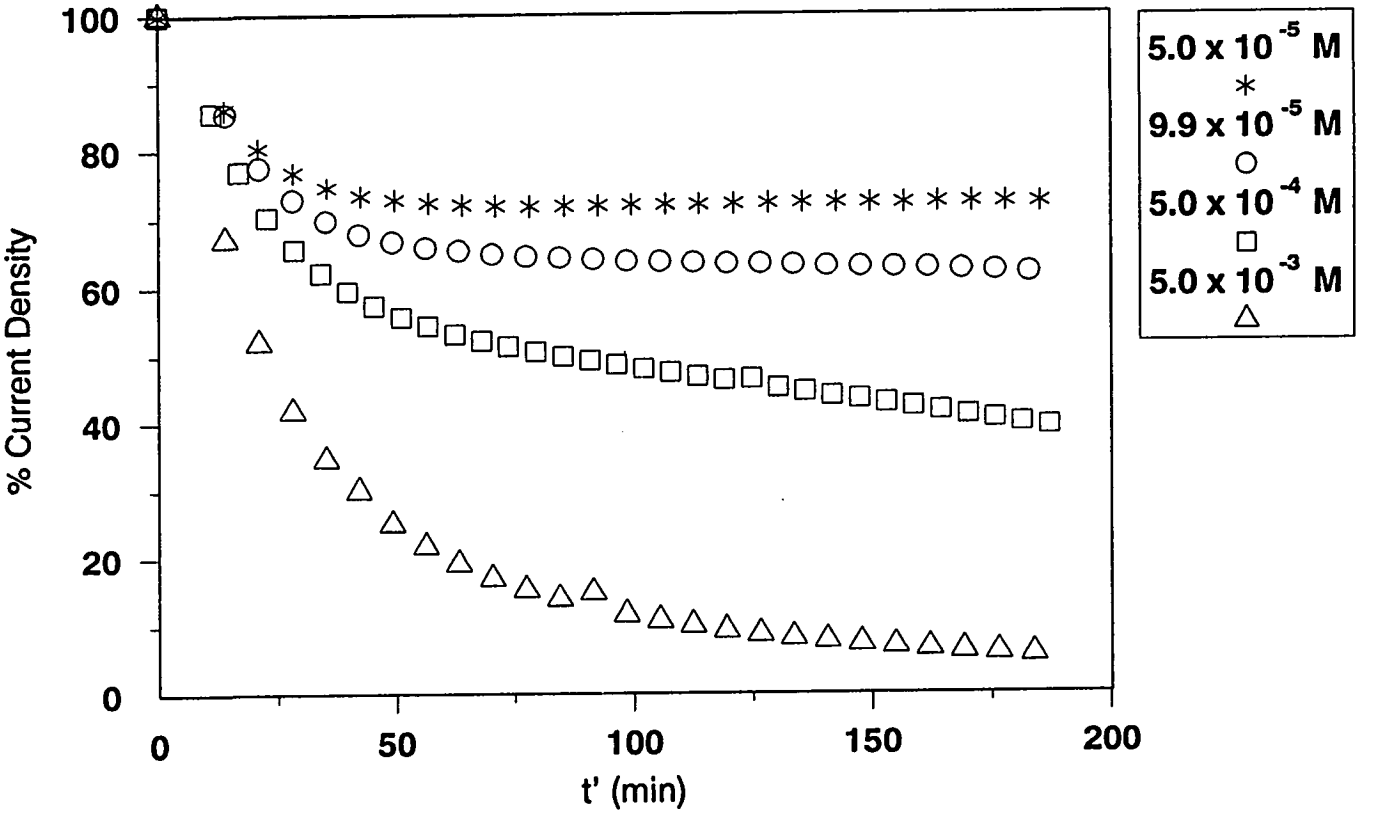

FIGURE 23. NORMALIZED PERMEATION CURVES FOR DIFFERENT CONCENTRATIONS OF HEXAMETHYLENE DIAMINE. THE CURRENT DENSITY AT THE INSTANT OF INHIBITOR ADDITION (t'=0) IS ASSIGNED THE VALUE 100.

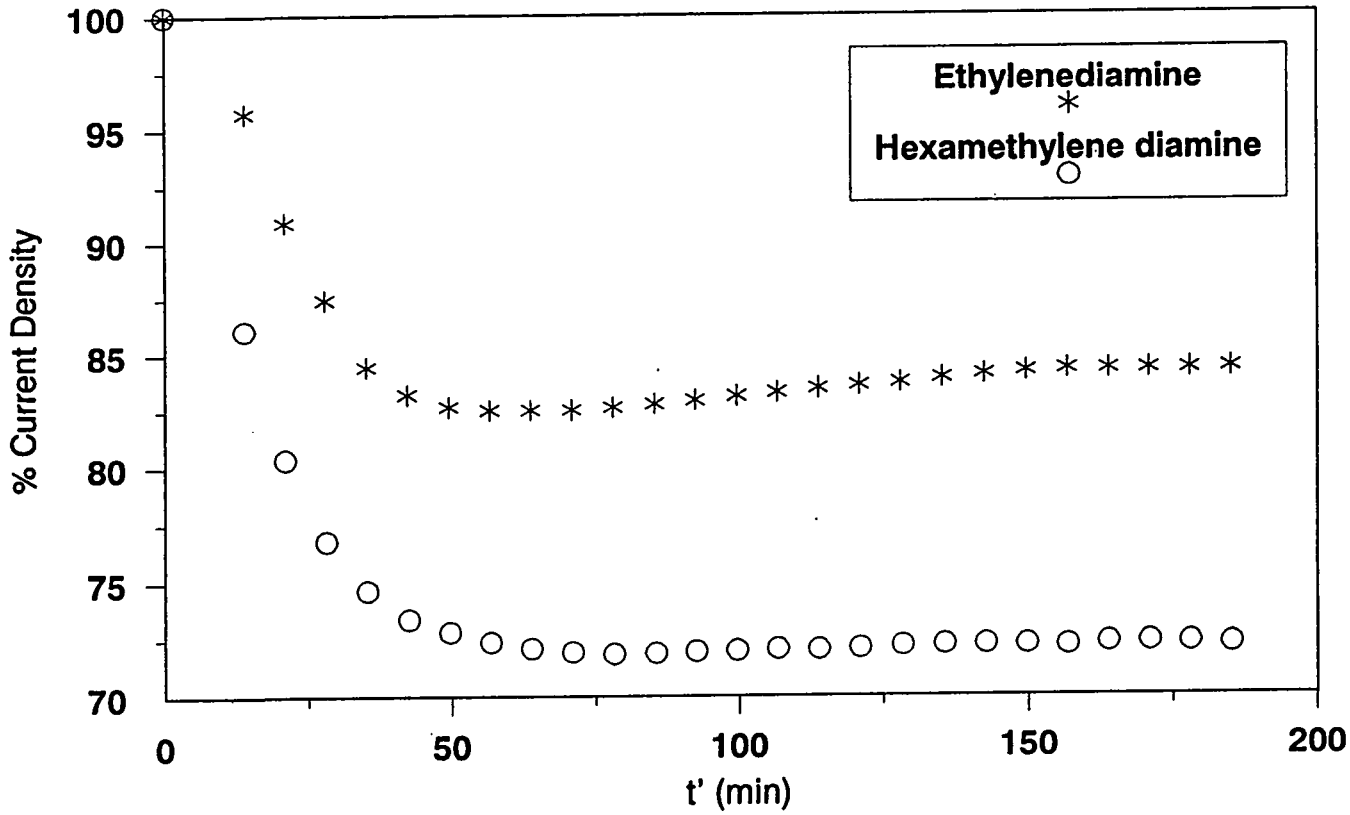

FIGURE 24. NORMALIZED PERMEATION CURVES FOR $5x10^{-5}$ M SOLUTIONS OF ETHYLENE-DIAMINE AND HEXAMETHYLENE DIAMINE. THE CURRENT DENSITY AT THE INSTANT OF INHIBITOR ADDITION (t'= 0) IS ASSIGNED THE VALUE 100.

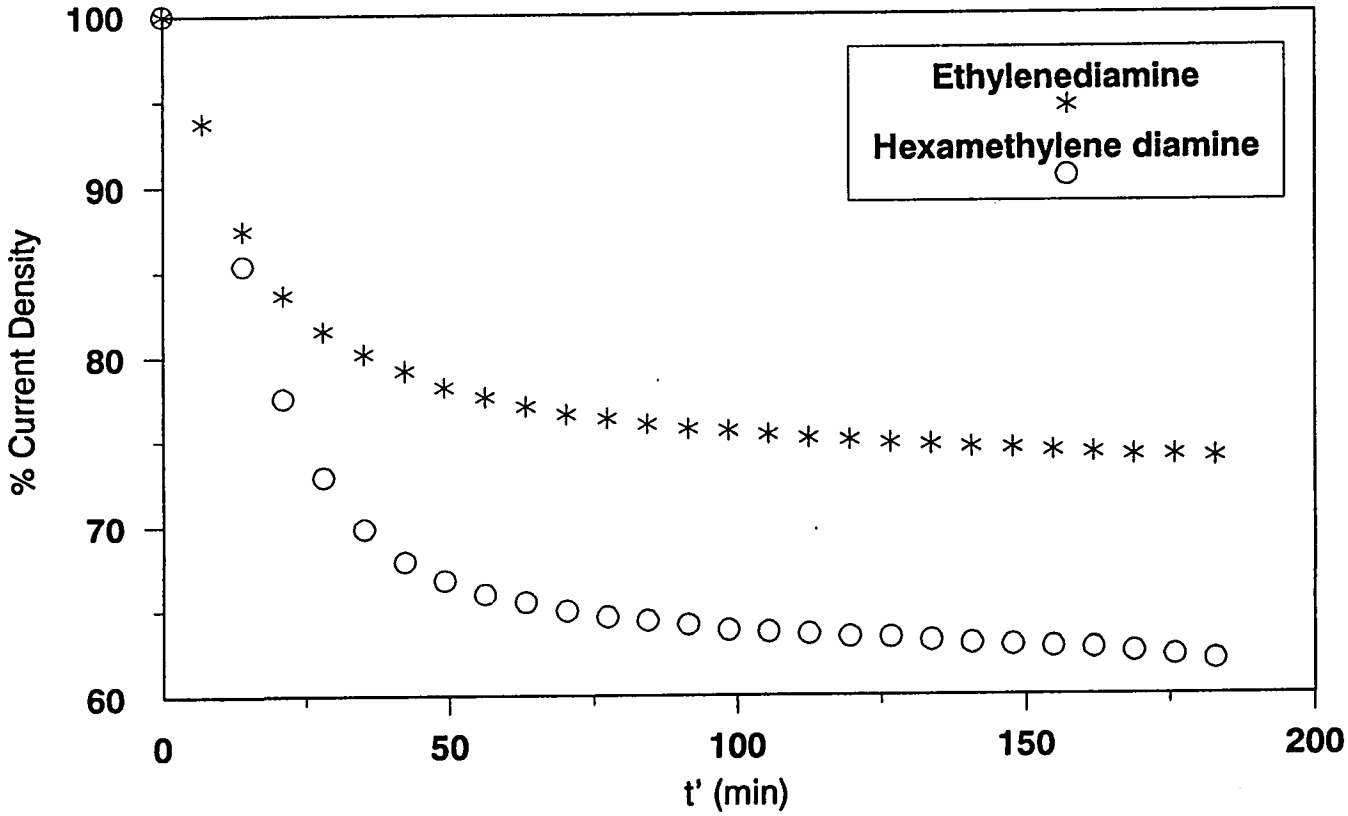

FIGURE 25. NORMALIZED PERMEATION CURVES FOR $1x10^{-4}$ M SOLUTIONS OF ETHYLENE-DIAMINE AND HEXAMETHYLENE DIAMINE. THE CURRENT DENSITY AT THE INSTANT OF INHIBITOR ADDITION (t'= 0) IS ASSIGNED THE VALUE 100.

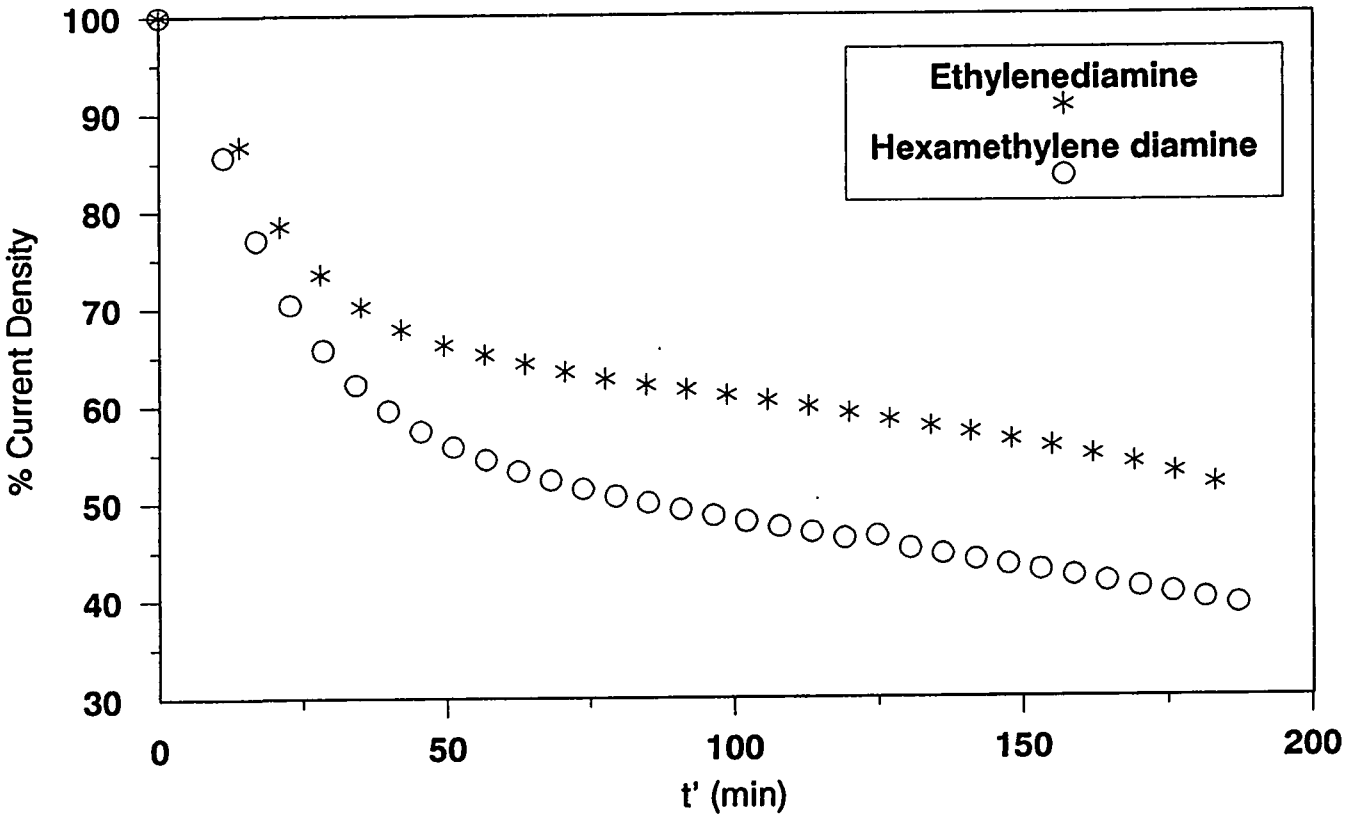

FIGURE 26. NORMALIZED PERMEATION CURVES FOR $5x10^{-4}$ M SOLUTIONS OF ETHYLENE-DIAMINE AND HEXAMETHYLENE DIAMINE. THE CURRENT DENSITY AT THE INSTANT OF INHIBITOR ADDITION (t'= 0) IS ASSIGNED THE VALUE 100.

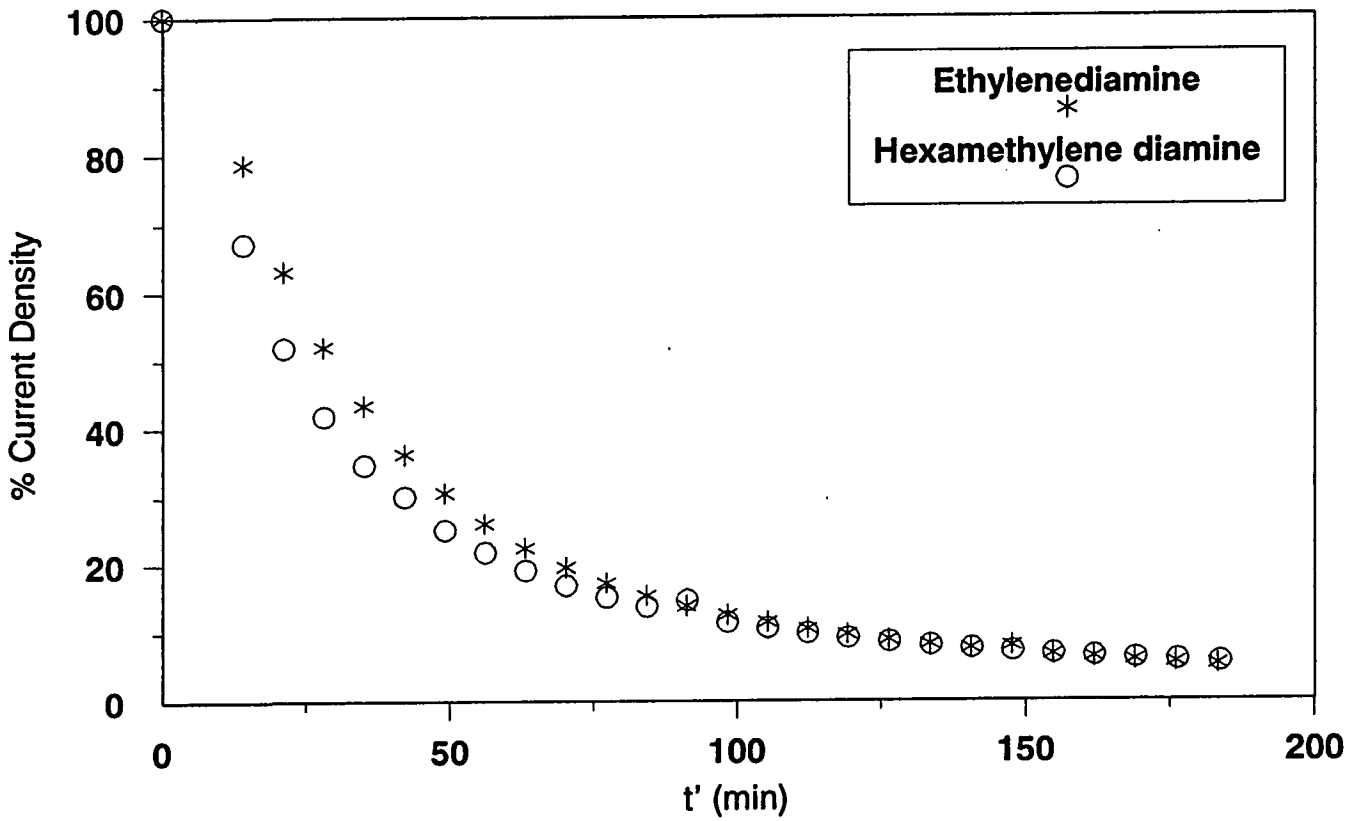

FIGURE 27. NORMALIZED PERMEATION CURVES FOR $5x10^{-3}$ M SOLUTIONS OF ETHYLENE-DIAMINE AND HEXAMETHYLENE DIAMINE. THE CURRENT DENSITY AT THE INSTANT OF INHIBITOR ADDITION (t'= 0) IS ASSIGNED THE VALUE 100.

than the electrons at the two nitrogens of EDA because of the higher number of the electron donating methylene groups in the former. Moreover, the higher number of the methylene groups induces a higher hydrophobicity in HMDA and increases its projected inhibitor molecular area, thereby making it a more effective inhibitor[28,34] than EDA.

Figure 28 shows the |slope| versus concentration curves for ethylenediamine and hexamethylene diamine. At sufficiently high concentrations of either EDA or HMDA, the surface becomes almost completely covered and the two compounds would display similar behavior. Figure 28 shows limiting concentrations for EDA and HMDA beyond which inhibition effectiveness increases very slightly with inhibitor concentration.

Figure 29 compares the hydrogen penetration inhibition behaviors of NaOH and the five amine compounds at 5×10^{-4} M and clearly demonstrates that the inhibition of hydrogen entry by the amine compounds is not due solely to raising the pH of the medium since NaOH, the strongest base, is a much less effective inhibitor than the weaker amine bases.

5.5.6 Reproducibility

To test for reproducibility duplicate runs were carried out on each of the 5×10^{-4} M solutions of morpholine and hexamethylene diamine respectively. The reproducibility of the normalized permeation curves for these solutions is illustrated in Figures 30 and

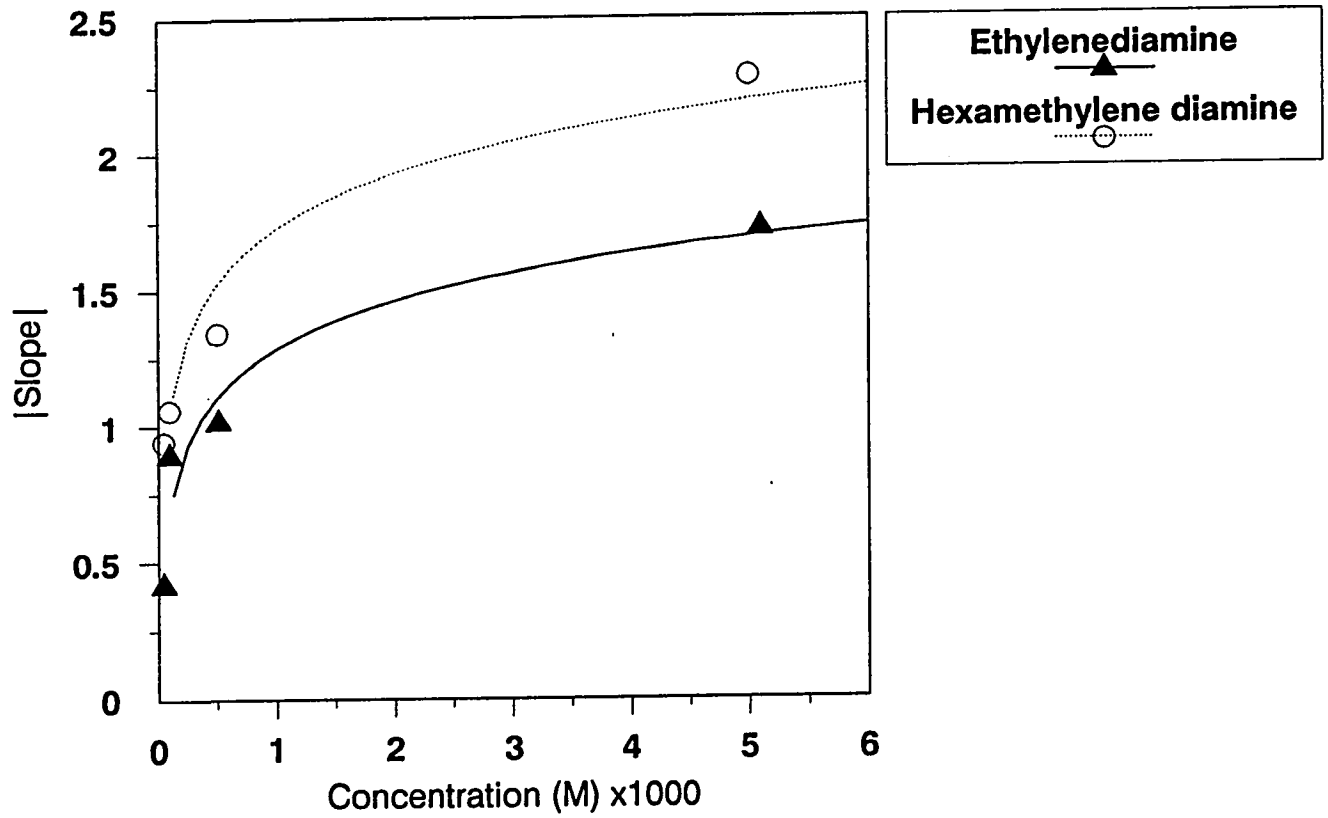

FIGURE 28. |SLOPE| VERSUS CONCENTRATION CURVES FOR ETHYLENEDIAMINE AND HEXAMETHYLENE DIAMINE. SLOPES WERE DETERMINED FROM THE FIRST THREE POINTS FOR EACH CONCENTRATION.

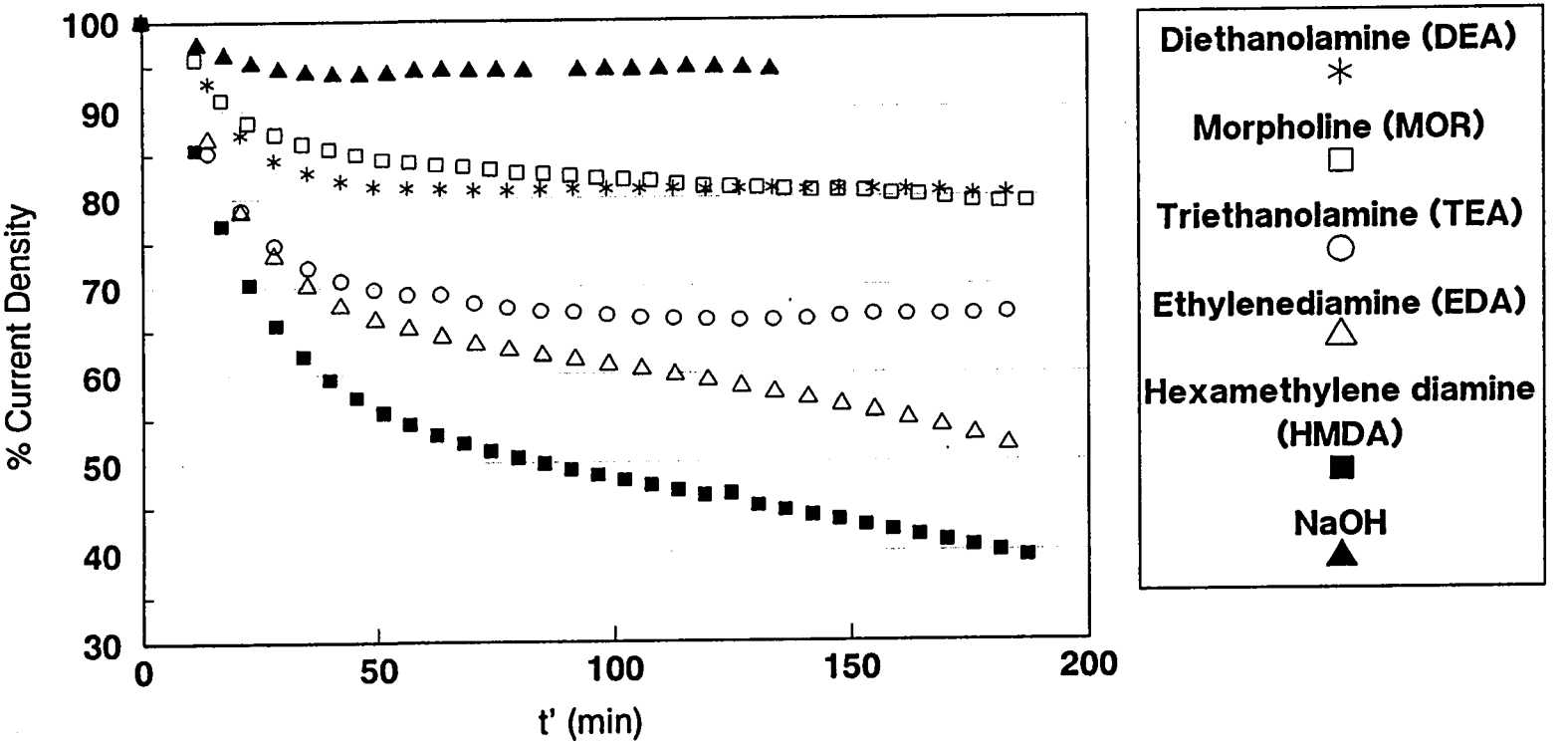

FIGURE 29. NORMALIZED PERMEATION CURVES FOR $5x10^{-4}$ M SOLUTIONS OF DEA, MOR, TEA, EDA, HMDA, AND NaOH. THE CURRENT DENSITY AT THE INSTANT OF INHIBITOR ADDITION (t'= 0) IS ASSIGNED THE VALUE 100.

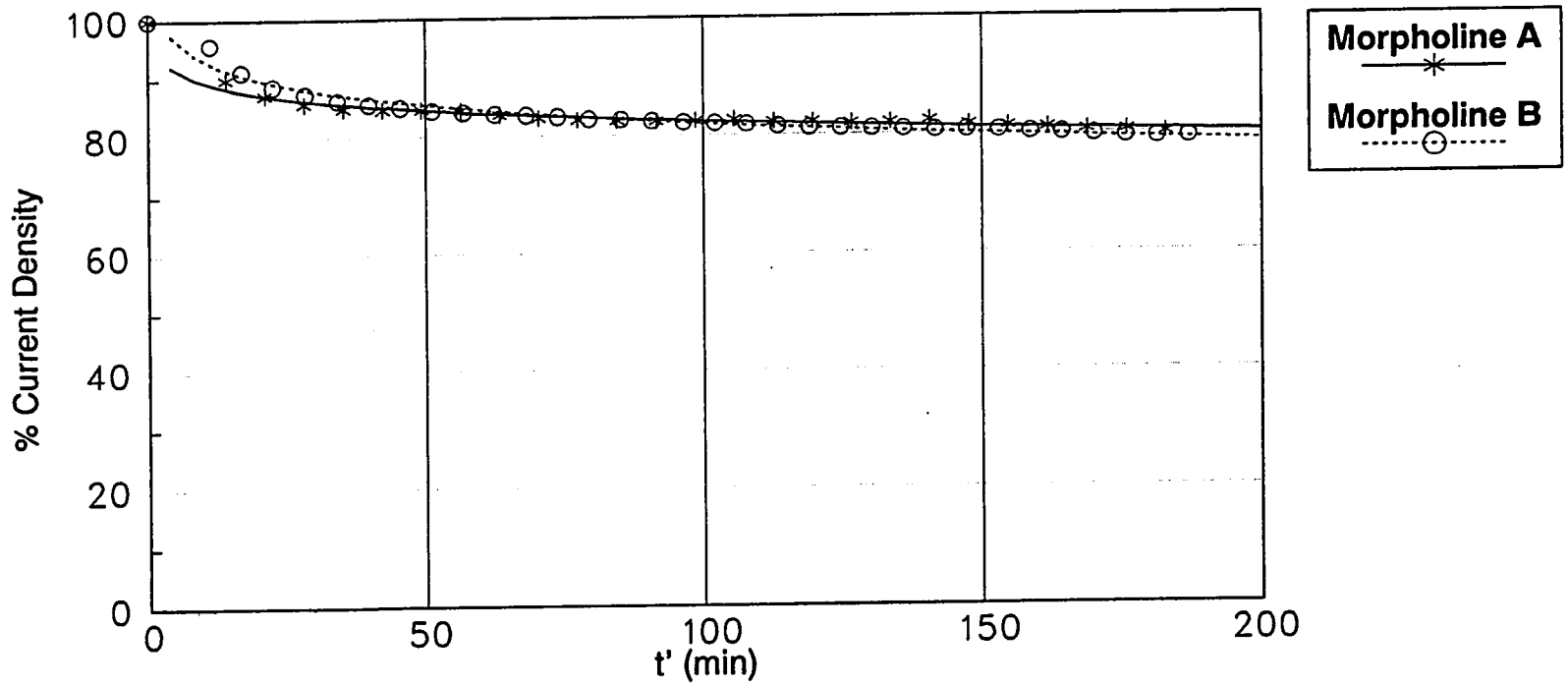

FIGURE 30. NORMALIZED PERMEATION CURVES FOR 5.2×10^{-4} M SOLUTIONS OF MORPHOLINE OBTAINED IN TWO DIFFERENT EXPERIMENTS. THE CURRENT DENSITY AT THE INSTANT OF INHIBITOR ADDITION (t'= 0) IS ASSIGNED THE VALUE 100.

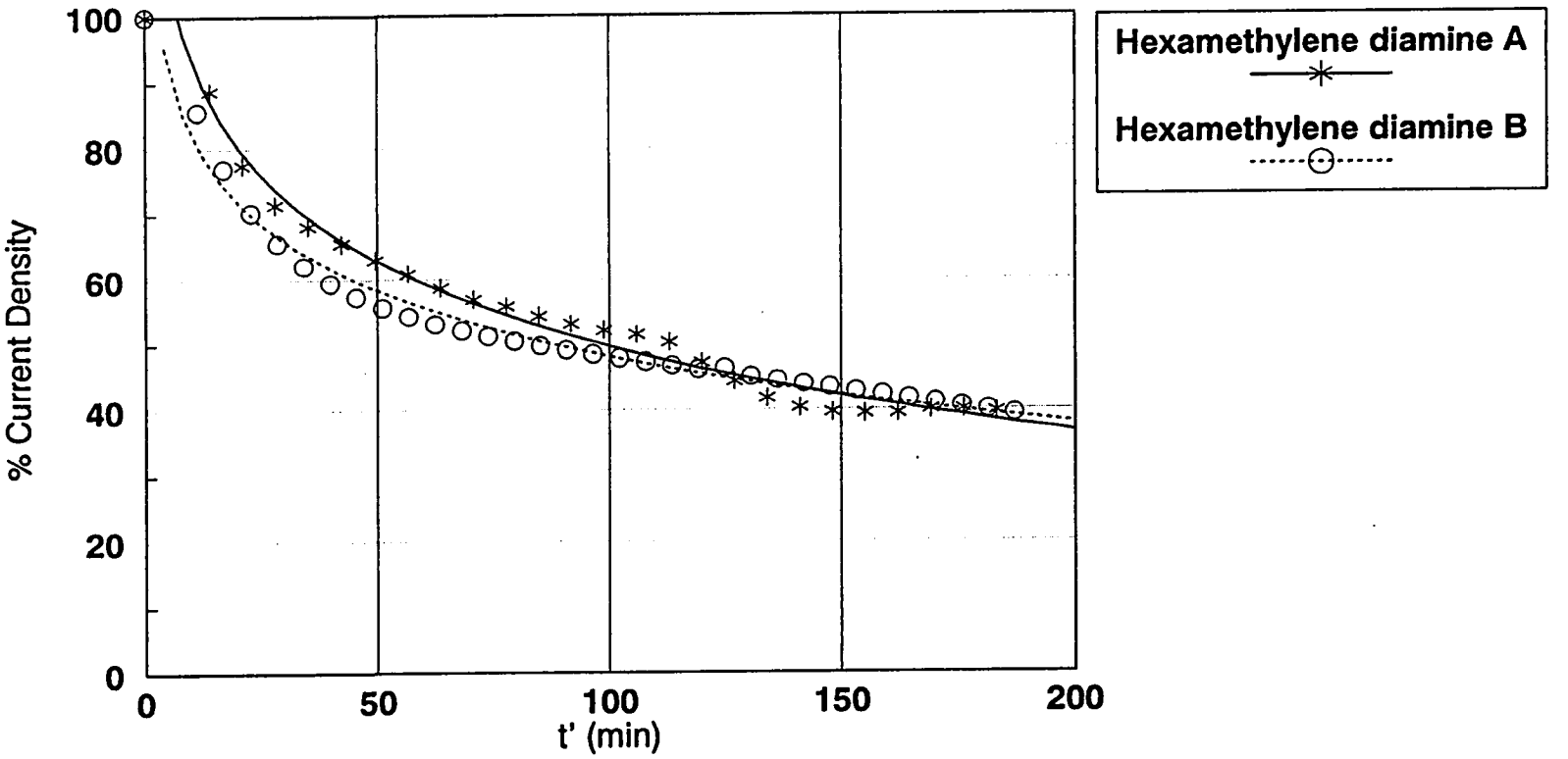

FIGURE 31. NORMALIZED PERMEATION CURVES FOR 5.0×10^{-4} M SOLUTIONS OF HEXAMETHYLENE DIAMINE OBTAINED IN TWO DIFFERENT EXPERIMENTS. THE CURRENT DENSITY AT THE INSTANT OF INHIBITOR ADDITION (t'= 0) IS ASSIGNED THE VALUE 100.

31 respectively. These figures ascertain the good reproducibility of the electrochemical hydrogen permeation method and of the experimental procedures adopted in conducting this study.

5.6 Diffusion Coefficients

Using the time-lag ($D_{0.63}$) and the Laplace ($D_{0.5}$) methods, hydrogen diffusion coefficients were determined for five different steel membranes, and the results are givenin Table 8. Table 8 demonstrates the good order of magnitude agreement among the values of the hydrogen diffusion coefficients in different steel membranes using the time-lag and the Laplace methods. The value obtained by the time-lag method, $(2.1\pm0.4)\times10^{-7}$ cm^2/sec, compares very well with the value of $(3.24\pm0.45)\times10^{-7}$ cm^2/sec obtained for iron in an earlier study[77] also using the time-lag method. Moreover, the value obtained by the Laplace method, $(1.2\pm0.2)\times10^{-7}$ cm^2/sec compares very well with values ranging from 2.0×10^{-7} to 3.3×10^{-7} cm^2/sec obtained for iron in an earlier study[70] also using the Laplace method.

Based on their study of the variation of D with membrane thickness Wach et al.[85] proposed the formation of a barrier to hydrogen diffusion. On the basis of their proposition they derive the relation

$$D_{Recal} = D_{eff} \times \frac{(L + \Delta L)^2}{L^2}$$

(where D_{eff} and D_{Recal} are the effective and the recalculated diffusion coefficients), for the recalculation of effective diffusion coefficients. In this equation ΔL is the assumed increment in the membrane thickness L and was given the values 0.1 and 0.05 cm respectively when hydrogen was introduced electrolytically or by other means. Table 9 shows the good comparison between typical values of effective and recalculated diffusion coefficients, extracted from a list in the paper of Wach et al.[85] and the values obtained in this study.

TABLE 8

Hydrogen Diffusion Coefficients, in Five Steel Membranes, Determined by the Time-lag ($D_{o.63}$) and the Laplace ($D_{o.5}$) Methods.

$i_{d,max}$ ($\mu A/cm^2$)	$D_{0.63}$ (cm^2/sec)	$D_{0.5}$ (cm^2/sec)
39.6	2.5×10^{-7}	1.4×10^{-7}
38.9	2.4×10^{-7}	1.4×10^{-7}
41.1	2.0×10^{-7}	1.2×10^{-7}
35.3	1.8×10^{-7}	1.0×10^{-7}
28.9	1.6×10^{-7}	9.3×10^{-8}
AVERAGE	2.1×10^{-7}	1.2×10^{-7}
STANDARD DEVIATION	0.4×10^{-7}	0.2×10^{-7}

TABLE 9

Effective and Recalculated Values of the Hydrogen Diffusion Coefficient in Steel, Using the Method of Wach et al.[85]

	Membrane Thickness, L (cm)	Effective D ($cm^2.Sec^{-1}$)	Recalculated D ($cm^2.Sec^{-1}$)	Material	ΔL (cm)
From Ref. 85	0.008	9.2×10^{-10}	1.5×10^{-6}	0.5C Steel	-
	0.076	-	0.5×10^{-6}	Mild Steel	-
	0.012	1.4×10^{-8}	1.2×10^{-6}	Mild Steel	-
	0.02	3.8×10^{-7}	5.2×10^{-6}	Mild Steel	-
	0.042	2.0×10^{-6}	1.0×10^{-6}	Mild Steel	-
	0.16	2.0×10^{-6}	5.2×10^{-6}	Mild Steel	-
	0.10	2.8×10^{-6}	1.1×10^{-5}	Mild Steel	-
	0.0254	2.3×10^{-8}	5.6×10^{-7}	Mild Steel	-
From This Study	0.079	$(2.1\pm0.4)\times10^{-7}$	$(1.1\pm0.2)\times10^{-6}$	Mild Steel	0.1
	0.079	-	$(5.6\pm1.0)\times10^{-7}$	Mild Steel	0.05
	0.079	$(1.2\pm0.2)\times10^{-7}$	$(6.2\pm1.0)\times10^{-7}$	Mild Steel	0.1
	0.079	-	$(3.2\pm0.5)\times10^{-7}$	Mild Steel	0.05

CHAPTER 6

CONCLUSIONS

6.1 The Electrochemical Hydrogen Permeation System

An electrochemical hydrogen permeation system was successfully designed, constructed, and characterized. An anodic potential of -200 mV versus Pt reference electrode was selected and used throughout the course of this study. To evaluate the reliability of our system diffusion coefficient of hydrogen atoms in API A106 grade B steel membranes was determined. It was found to be 1.2 to 2.1×10^{-7} cm^2/sec which compares very well with literature values for mild steel thereby establishing the reliability of our system. Bare steel membranes gave a lower $i_{d,max}$ than the membranes which were electroplated with palladium. This is attributable to passivation of the anodic side in the bare steel membrane. For this reason the membranes used in our study were electroplated with palladium on the anodic side.

Hydrogen permeation curves with and without a characteristic hump, resulting from exceeding the critical hydrogen atom concentration in steel, were observed. The decay transient after the hump was not as fast as that in previously reported hydrogen permeation curves. This was attributed to a conversion process involving a sulfide layer

that opposes the decay transient. Moreover, although blistering was observed visually in some membranes, the characteristic hump was not present in the corresponding permeation curves. This suggests that trapping sites other than voids and microvoids are responsible for this hump.

6.2 Organic Amines Evaluation

Consecutive additions of the amines to the corrosive media gave unmanageable results, for comparing the same chemical at different concentrations or for comparing different chemicals at the same concentration, as a result of modification of the membrane surface by the addition of the chemicals.

The instantaneous decay transient due to the addition of a chemical, after the hydrogen permeation flux reaches a steady-state beyond the characteristic hump, was attributed to a lowering of H^+ mobility, a decrease in the HS^- diffusion coefficient in the double layer region (brought about by an increase in its effective hydrodynamic radius), interface chemisorption, and the formation of an interphase layer.

A so called 'secondary hydrogen diffusion process' superimposed on the process responsible for the instantaneous decay transient is postulated to explain the leveling of the hydrogen permeation curve. This process possibly involves a decrease in hydrogen atom activity in the steel membrane to the extent that weakly or reversibly trapped

hydrogen atoms diffuse out, an increase in the pH (established by the continuous purging with H_2S gas) after amine addition and by a flaking-off process as a consequence of the formation of a thick and poorly oriented (packed) interphase layer.

Diethanolamine (DEA), morpholine (MOR), and triethanolamine (TEA) were found, under the conditions used in this study, to retard hydrogen entry and until a critical concentration limit is reached the effectiveness of hydrogen entry inhibition increases as the inhibitor concentration increases. At low concentrations, the order of the effectiveness of hydrogen entry inhibition follows the trend: DEA < MOR < TEA. This trend was rationalized on the basis of (i) the availability of electrons at the nitrogen reaction center, (ii) the number of carbon atoms, (iii) the projected molecular area of the inhibitor and (iv) hydrophobicity. At higher concentrations the inhibition effectiveness of these three chemicals becomes comparable. Intramolecular hydrogen-bonding present in DEA and to a lesser extent in TEA, and increased surface coverage with inhibitor concentration may be responsible for this behavior.

Ethylenediamine (EDA) and hexamethylene diamine (HMDA) were also found to retard hydrogen entry and again up to a critical concentration limit, hydrogen entry inhibition increases as the inhibitor concentration increases. At low concentrations HMDA is more effective at inhibiting hydrogen entry than EDA. This was attributed to the greater availability of electrons on the two nitrogen atoms in HMDA than on the two nitrogen atoms in EDA due to the greater number of electron donating methylene groups

in HMDA and to the greater hydrophobicity of HMDA. At sufficiently high concentrations EDA and HMDA display similar behavior. This is attributed to a complete or near complete coverage of the surface of the steel membrane.

REFERENCES

1. R. N. Tuttle and R.D. Kane, eds., "H_2S Corrosion in Oil and Gas Production - A compilation of Classic Papers", NACE (1981).

2. M. H. Bartz and C. E. Rawlins, *Corrosion* **4**, 187 (1948).

3. M. Zamanzadeh, R. N. Iyer and H. W. Pickering, Paper No.208, Corrosion/90, NACE (1990).

4. A. V. Shreider, *Zashch. Met.* **26**, No.2, 179 (1990).

5. R. D. Merrick, *Materials Performance* **28**, No. 2, 53 (1989).

6. J. O'M, Bockris and A. K. N. Reddy, "Modern Electrochemistry", Vol. 2, Plenum Press, New York, (1977), pp. 1231-1251.

7. R. D. McCright, "stress corrosion Cracking and Hydrogen Embrittlement of Iron Base Alloys", NACE, (1977), PP. 306-325, and references 5, 6, and 7, therein.

8. B. D. Craig, "Fundamental Aspects Corrosion Films in Corrosion Science", Plenum Press, New York, (1991), pp. 129-163.

9. M. A. V. Devanathan and Z. Stachurski, *J. Electrochem Soc.* **111**, 619 (1964).

10. a) J. McBreen, L. Nanis and W. Beck, *J. Electrochem. Soc.* **113**, 1218 (1966). b) L. Cailletet, Compt. Rend. 58, 327 (1864).

11. J. O'M. Bockris and A. K. N. Reddy, "Modern Electrochemistry", Vol. 2, Plenum Press, New York, 1977), pp. 1328-1350.

12. G. Alefeld and J. Völkl, eds., "Hydrogen in Metals I and II", Springer-Verlag, New York, (1978).

13. W. Beck, J. O'M. Bockris, J. McBreen and L. Nanis, *Proc. Roy. Soc.* **A290**, 220 (1966).

14. T. P. Radhakrishanan and L.L. Shreir, *Electrochim. Acta* **12**, 889 (1967).

15. J. O'M. Bockris, M.A. Genshaw and M. Fullenwider, *Electrochim. Acta* **15**, 47 (1970).

16. T. K. G. Namboodhiri and L. Nanis, *Acta met.* **21**, 663 (1973).

17. R. A. Oriani, *Acta met.* **1B**, 147 (1970).

18. G. M. Pressouyre, "The Role of Trapping on Hydrogen Transport and Embrittlement", Ph.D. Thesis, Carnegie - Mellon University, (1977) pp. 33-41.

19. L. Coudreuse and J. Charles, *Corros. Sci.* **27**, 1169 (1987).

20. J. O'M. Bockris in "Stress Corrosion Cracking and Hydrogen embrittlement of Iron Base alloys", R. W. Staehle, J. Hockmann, R. D. McCright and J. E. Slater, eds., NACE, (1977) pp. 286-305.

21. R. D. McCright and R. W. Staehle, *J. Electrochem. Soc.* **121**, 609 (1974).

22. M. A. V. Devanathan, Z. Stachurski and W. Beck, *J. Electrochem. Soc.* **110**, 886 (1963).

23. D. D. MacDonald, B. Robertsand J.B. Hyne, *Corros. Sci.* **18**, 411 (1978).

24. D. W. Shoesmith, P. Taylor, M. G. Bailey and D.G. Owen, *J. Electrochem. Soc.* **127**, 1007 (1980).

25. G. Schmitt, Corrosion/90, Paper No. 39, NACE, Las Vegas, (1990).

26. N. I. Podobaev and A. N. Kozlov, *Zashch. Met.* **22**, No. 3, 371 (1986).

27. B. D. Craig, "Fundamental Aspects Corrosion Films in Corrosion Science", Plenum Press, New York, (1991), pp. 47-88.

28. G. Trabanelli and V. Carassiti, "Mechanism and phenomenology of Organic Inhibitors", in: Advances in Corrosion Science and Technology, Vol.1, M.G. Fontanna and R.W. Staehle, eds., Plenum Press, New York, (1970), pp. 147-228.

29. W. J. Lörenz and F. Mansfeld, in: "Corrosion Inhibition", R. H. Hausler,ed., NACE, Texas (1988), pp. 7-13.

30. N. Hackerman, *Corrosion* **18**, 332t (1962) September.

31. B. D. Craig, "Fundamental Aspects of Corrosion Films in Corrosion Science", Plenum Press, new York, (1991), pp. 89-108.

32. I. L. Rosenfeld, *Corrosion* **37**,371 (1981).

33. H. Kaesche and N. Hackerman, *J. Electrochem. Soc.* **105**, 191 (1958).

34. P. Dupin, D. A. Viloria-Vera, A. de Savignac, A. Lattes, B. Sutter and Ph. Haicour, Proc. 5th Europ. Symp. Corros. Inhibitors, Vol. 1, p. 301, Universita delgi Studi di Ferrara, Ferrara, Italy (1980).

35. S. N. Raicheva, B. V. Aleksiev and E. I. Sokolova, *Corros. Sci.* **34**, No.2, 343 (1993).

36. P. F. Cox., R. L. Every and O. L. Riggs, Jr., *Corrosion* **20**, 299t (1964) September.

37. C. C. Nathan, ed., "Corrosion Inhibitors", NACE, Texas, (1973) pp. 7-27.

38. Z. Szklarska-Smialowska, in: "Corrosion Inhibition", R. H. Hausler, ed., NACE, Texas, (1988), pp. 1-6.

39. Z. A. Iofa, *Zashch. Met.* **16**, No.3, 295 (1980).

40. F. M. Donahue, A. Akiyama and K. Nobe, *J. Electrochem. Soc.* **114**, 1006 (1967).

41. I. L. Rozenfel'd, L. V. Frolova, V. M. Brusnikina, N. E. Legezin and B. N. Al'tshuler, *Zashch. Met.* **17**, No.1, 43 (1981).

42. I. L. Rozenfel'd, D. B. Bogomolov, A. E. Gorodetskii, L. P. Kazanskii, L. V. Frolova and L. I. Shamova, *Zashch. Met.* **18**, No.2, 163 (1982).

43. M. K. Panov, M. D. Getmanskii, E. Kh. Enikeev and M. N. Fokin, *Zashch. Met.* **25**, No. 4, 555 (1989).

44. N. I. Podobaev and O. G. Barinov, *Zashch. Met.* **28**, No.1, 102 (1992).

45. M. K. Panov, M. D. Getmanskii, E. Kh. Enikeev and M. N. Fokin, *Zashch. Met.* **25**,815 (1989).

46. J. O'M. Bockris, J. McBreen and L. Nanis, *J. Electrochem. Soc.* **112**, 1025 (1965).

47. L. I. Antropov, M. A. Gerasimenko, Yu. S. Gerasimenko and Yu. A. Savgira, Extended Abstracts of Papers, Third International Congress on Metallic Corrosion, Moscow, May (1966), pp. 97-98.

48. A. Benbachir, A. Srhiri, K. Benchekroun, A. Elkholy and F. Dabosi, in: "Corrosion Inhibition", R. H. Hausler, ed., NACE, Texas (1988), pp. 127-131.

49. L. V. Frolova and K. M. Alieva, *Zashch. Met.* **25**, No.5, 824 (1989).

50. D. D. Singh, T. B. Singh, P. Chatterjee, B. B. Paty and K. P. Mukherjee, *Corr. Prev. Cont.*, 37 (1990) April.

51. R. L. Martin, Paper No. 152, Corrosion/92, NACE, April (1992).

52. C. Jacklin, *Corrosion* **9**, 1 (1953).

53. C. Jacklin, *Trans. ASME* 77, 449 (1955).

54. R. R. Annand, R. M. Hurd and N. Hackerman, *J. Electrochem. Soc.* **112**, 144 (1965).

55. V. G. Starchak and L. D. Kosukhina, *Zashch. Met.* **25**, No.1, 143 (1989).

56. M. A. V. Devanathan and L. Stachurski, *Proc. Roy. Soc.* (London) **A270**, 90 (1962).

57. M. A. Fullenwider, "The Electro-permeation of Hydrogen in Metals", Ph.D. Thesis, University of Pennsylvania, (1969).

58. M. A. Fullenwider, "Hydrogen Entry and Action in Metals", Pergamon Press, New York, (1983).

59. V. Breger and E. Gileadi, *Electrochim. Acta* **16**, 177 (1971).

60. J. O'M. Bockris, in: "Atomistics of Fracture", R.M. Latanision and J.R. Pickens, eds., Plenum Press, New York (1983), pp. 593-601.

61. A. Turnbull, M. Maria and N. D. Thomas, *Corros. Sci.* **29**, No.1, 89 (1989) and references therein.

62. W. Beck, J. O'M. Bockris, M. A. Genshaw and P. K. Subramanyan, *Met. Trans.* **2**, 883 (1971).

63. A. J. Kumnick and H. H. Johnson, *Met. Trans.* **5**, 1199 (1974).

64. A. J. Kumnick and H. H. Johnson, *Met. Trans A.* **6A**, 1087 (1975).

65. A. J. Kumnick and H. H. Johnson, *Acta Metall.* **28**, 33 (1980).

66. Ruey-Way Lin and H. H. Johnson, in: "Advanced Techniques for Characterizing Hydrogen in Metals", N. F. Fiore and B. J. Berkowitz, eds., The Metallurgical Society of AIME, New York, (1982), pp. 105-118.

67. M. Surkein and R. Heidersbach, in: "Advanced Techniques for Characterizing Hydrogen in Metals", N. F. Fiore and B. J. Berkowitz, eds., The Metallurgical Society of AIME, New York, (1982), pp. 119-132.

68. D. A. Berman, W. Beck and J. J. Deluccia, in: "Hydrogen in Metals", I. M. Bernstein and A. W. Thompson, eds. ASM, Ohio, (1974), pp. 595-607 and references therein.

69. R. L. Martin, *Materials Performance,* 21 (1974) July.

70. Z. Jiashen and Z.Jingmao, *Corrosion* **49**, No.3, 256 (1993).

71. E. M. Moore Jr., *J. Pet. Tech.*, 613 (1984) April, and references therein

72. "Worldwide Guide to Equivalent Irons and Steels", ASM, Ohio, (1979), p. 134.

73. "Handbook of Comparative World Steel Standards", Vol. 6, The International Technical Information Institute, Tokyo, Japan (1980), p. II-42.

74. Y. T. Al-Janabi and A. L. Lewis, Paper No. 18, Proceedings of the 1990 Laboratories Department Technical Exchange Meeting, Saudi Aramco, Dhahran, (1990).

75. G. Perboni and G. Rocchini, in: "Corrosion Inhibition", R. H. Hausler, ed., NACE, Houston (1988), pp. 201-208.

76. M. G. Fontana and N. D. Greene, "Corrosion Engineering", McGraw-Hill, Inc., New York, (1978), pp. 10-18.

77. Su-Il Pyun and R. A. Oriani, *Corros. Sci.* **29**, 485 (1989).

78. A. M. Brass, A. Boutry-Forviell and M. Aucouturier, *J. Electrochem. Soc.* **139**, 374 (1992).

79. J. O'M. Bockris and P. K. Subramanyan, *J. Electrochem. Soc.* **118**, 1114 (1971).

80. I. M. Bernstein and A. W. Thompson, in: "Advanced Techniques for Characterizing Hydrogen in Metals", N. F. Fiore and B. J. Berkowitz, eds., The Metallurgical Society of AIME, New York, (1982) pp. 89-103.

81. R. M. Latanision, C. R. Compeau and M. Kurkela, in: "Hydrogen Embrittlement and Stress Corrosion Cracking", R. Gibala and R. F. Hehemann, eds., ASM, Ohio, (1984), pp. 297-313.

82. M. Kimura, N. Totsuka, T. Kurisu, T. Hane, and Y. Nakai, *Corrosion* 44, No. 10, 738 (1988).

83. P. W. Atkins, "Physical Chemistry", 4th ed., Oxford University Press, Oxford, (1990), pp. 748-773.

84. M. I. Luppo and J. Ovejero-Garcia, *Corros. Sci.* 32, No. 10, 1125 (1991).

85. S. Wach, A. P. Miodownik and J. Mackowiak, *Corros. Sci.* 6, 271 (1966), and references therein.

APPENDIX

CHEMICAL DATA SHEET

Chemical Name: **Diethanolamine**
Formula: $HN(CH_2CH_2OH)_2$
Merck Index Number: 3078
Molecula Weight: 105.14 g/mol
Boiling Point: 271 degrees C
Melting Point: 28 degrees C
Density: 1.0966 g/cm^3
Solubility: water, alcohol

Chemical Name: **Triethanolamine**
Formula: $N(CH_2CH_2OH)_3$
Merck Index Number: 9341
Molecular Weight: 149.19 g/mol
Boiling Point: 277 degrees C
Melting Point: 21-22 degrees C
Density: 1.1242 g/cm^3
Solubility: water, alcohol, chloroform
Comments: Very hygroscopic, viscous liquid, slight ammoniacal odor, turns brown on exposure to air and light, demulsifier.

Chemical Name: **Morpholine**
Formula: $HN(CH_2CH_2)_2O$
Merck Index Number: 6116
Molecular Weight: 87.12 g/mol
Boiling Point: 128.3 degrees C
Melting Point: -4.7 degrees C
Density: 1.0005 g/cm^3
Solubility: water, alcohol, ether, acetone, benzene
Comments: Corrosive to human skin, Hygroscopic, mobile liquid, characteristic amine odor.

Chemical Name: **Ethylenediamine**
Formula: $H_2NCH_2CH_2NH_2$
Merck Index Number: 3731
Molecular Weight: 60.11 g/mol
Boiling Point: 116.117 degrees C
Melting Point: 8.5 degrees C
Density: 0.8995 g/cm^3

APPENDIX "Continued": Chemical Data Sheet

Solubility: water, alcohol
Comments: Form hydrate with water, may absorb CO_2 from air to form a nonvolatile carbonate.

Chemical Name: **1,6- Diamino hexane or Hexamethylene diamine**
Formula: $H_2N(CH_2)_6NH_2$
Merck Index Number: 4564
Molecular Weight: 116.21 g/mol
Boiling Point: 204-205 degrees C
Melting Point: 41-42 degrees C
Solubility: water, alcohol, benzene
Comments: Absorb H_2O and CO_2 from air.